HHS Public Access

Author manuscript

*Neuron*. Author manuscript; available in PMC 2017 April 06.

Published in final edited form as:

*Neuron*. 2016 April 6; 90(1): 56–69. doi:10.1016/j.neuron.2016.02.040.

# GABAergic neuron-specific loss of *Ube3a* causes Angelman syndrome-like EEG abnormalities and enhances seizure susceptibility

**Matthew C. Judson**[1,3,#], **Michael L. Wallace**[2,3,‡,#], **Michael S. Sidorov**[1,3], **Alain C. Burette**[1], **Bin Gu**[1,3], **Geeske M. van Woerden**[4,5], **Ian F. King**[6], **Ji Eun Han**[1], **Mark J. Zylka**[1,2,3,7], **Ype Elgersma**[4,5], **Richard J. Weinberg**[1,2], and **Benjamin D. Philpot**[1,2,3,7,*]

[1]Department of Cell Biology and Physiology, University of North Carolina, Chapel Hill, 27599-7545 [2]Curriculum in Neurobiology, University of North Carolina, Chapel Hill 27599-7250 [3]Carolina Institute for Developmental Disabilities, University of North Carolina, Chapel Hill, 27599-7255 [4]Department of Neuroscience, Erasmus Medical Center, Wytemaweg 80, NL-3015 CN Rotterdam, the Netherlands [5]ENCORE Center for Neurodevelopmental Disorders, Erasmus Medical Center, Rotterdam, Wytemaweg 80, 3015 CN, the Netherlands [6]Department of Pathology and Laboratory Medicine, University of North Carolina, Chapel Hill, 27599-7525 [7]Neuroscience Center, University of North Carolina, Chapel Hill, 27599-7250

## SUMMARY

Loss of maternal *UBE3A* causes Angelman syndrome (AS), a neurodevelopmental disorder associated with severe epilepsy. We previously implicated GABAergic deficits onto layer (L) 2/3 pyramidal neurons in the pathogenesis of neocortical hyperexcitability, and perhaps epilepsy, in AS model mice. Here we investigate consequences of selective *Ube3a* loss from either GABAergic or glutamatergic neurons, focusing on the development of hyperexcitability within L2/3 neocortex and in broader circuit and behavioral contexts. We find that GABAergic *Ube3a* loss causes AS-like

*Correspondence: bphilpot@med.unc.edu.
‡Present address: Department of Neurobiology, Harvard Medical School, Boston, 02115
#These authors contributed equally to this work



**SUPPLEMENTAL INFORMATION**

Supplemental information includes Supplemental Figures 1–8, Supplemental Table 1, Supplemental Experimental Procedures, Author Contributions, and Supplemental References, which can be found with this article online.

**AUTHOR CONTRIBUTIONS**

M.J. generated and molecularly characterized *Ube3a*$^{FLOX}$ mice, and designed and performed light microscopy, whole-cell electrophysiology, and behavioral seizure experiments. M.W. designed and performed whole-cell electrophysiology and audiogenic seizure experiments. M.S. designed and performed *in vivo* electrophysiology experiments. A.B. designed and performed electron microscopy experiments. B.G. designed and performed flurothyl seizure experiments. G.v.W. advised on *Ube3a*$^{STOP/p+}$ experiments. I.K. performed qRT-PCR experiments. J.H. performed light microscopic analyses. M.Z. advised on qRT-PCR experiments. Y.E. advised on *Ube3a*$^{STOP/p+}$ experiments. R.W. designed experiments. B.P. designed experiments. M.J, M.W, R.W, and B.P wrote the manuscript, which was edited by all co-authors.

**COMPETING INTERESTS STATEMENT**

The authors declare that they have no competing financial interests.

increases in neocortical EEG delta power, enhances seizure susceptibility, and leads to presynaptic accumulation of clathrin-coated vesicles (CCVs) – all without decreasing GABAergic inhibition onto L2/3 pyramidal neurons. Conversely, glutamatergic *Ube3a* loss fails to yield EEG abnormalities, seizures, or associated CCV phenotypes, despite impairing tonic inhibition onto L2/3 pyramidal neurons. These results substantiate GABAergic *Ube3a* loss as the principal cause of circuit hyperexcitability in AS mice, lending insight into ictogenic mechanisms in AS.

## INTRODUCTION

Angelman syndrome (AS) is a debilitating neurodevelopmental disorder defined by severe developmental delay, movement disorders, profound speech impairment, and highly penetrant electroencephalographic (EEG) abnormalities and seizures (Williams et al., 2006; Thibert et al., 2013). The frequency, severity, and intractability of the seizures exact a heavy toll on the quality of life of individuals with AS and their caregivers (Thibert et al., 2013). Loss of function of the maternal *UBE3A* allele causes AS (Kishino et al., 1997; Matsuura et al., 1997; Sutcliffe et al., 1997). *UBE3A* encodes an E3 ubiquitin ligase, which catalyzes the transfer of ubiquitin to substrate proteins, thereby targeting them for proteasomal degradation or otherwise altering their localization or function (Rotin and Kumar, 2009; Mabb and Ehlers, 2010; Mabb et al., 2011). Because mutations that selectively inhibit UBE3A ligase activity are sufficient to cause AS, improper ubiquitin substrate regulation likely contributes to the pathogenesis of the disorder (Cooper et al., 2004). Unlike other cells, neurons express UBE3A exclusively from the maternal allele due to evolutionary conserved, cell type-specific epigenetic mechanisms that silence the paternal *UBE3A* allele (Rougeulle et al., 1997; Yamasaki et al., 2003; Judson et al., 2014). Accordingly, neurons are especially vulnerable to loss of maternal *UBE3A*.

Previously, we utilized a maternal *Ube3a* null (*Ube3a*$^{m-/p+}$) mouse model of AS (Jiang et al., 1998) to explore the neural basis of hyperexcitability phenotypes in the disorder. We discovered that severe reduction of inhibitory GABAergic input to layer (L) 2/3 pyramidal neurons outweighs corresponding losses of excitatory glutamatergic input, possibly contributing to neocortical hyperexcitability. Recovery of inhibitory synaptic transmission following high-frequency stimulation is severely compromised and is associated with accumulations of clathrin-coated vesicles (CCVs) at GABAergic presynaptic terminals onto L2/3 pyramidal neurons (Wallace et al., 2012). Maternal *Ube3a* deficiency may thus disrupt presynaptic vesicle cycling in GABAergic neurons, possibly through the dysregulation of UBE3A substrates that directly or indirectly compromise clathrin-mediated endocytosis. Conversely, it is possible that loss of maternal *Ube3a* expression in glutamatergic neurons compromises the postsynaptic effects of GABA on L2/3 pyramidal neurons, thereby contributing to hyperexcitability within the microcircuit and throughout the brain. In support of this latter possibility, modulation of expression or activity levels of ARC or the calcium/calmodulin-dependent kinase type II-α subunit (CaMKII-α) - both of which are preferentially expressed by glutamatergic forebrain neurons - has been shown to rescue circuit hyperexcitability and seizures in *Ube3a*$^{m-/p+}$ mice (van Woerden et al., 2007; Mandel-Brehm et al., 2015). Thus, an immediate goal is to determine whether maternal *Ube3a* loss restricted to either GABAergic or glutamatergic neurons is sufficient to impair

GABAergic inhibition onto L2/3 pyramidal neurons, thereby leading to broader circuit-level and behavioral manifestations of hyperexcitability.

Here we utilize novel conditional *Ube3a* mouse models to identify the neurons and neural circuits underlying the pathogenesis of circuit hyperexcitability in AS. We focus on selective *Ube3a* loss from GABAergic or glutamatergic neurons, which are largely responsible for orchestrating the balance between excitation and inhibition in cerebral circuits. Our results provide compelling evidence that GABAergic, but not glutamatergic, *Ube3a* loss is responsible for mediating the EEG abnormalities and seizures that affect individuals with AS.

## RESULTS

### GABAergic *Ube3a* Loss Does Not Impair GABAergic Neurotransmission onto L2/3 Pyramidal Neurons

To enable genetic dissection of neuron type-specific contributions to circuit hyperexcitability in AS, we generated a novel mouse with maternal inheritance of a floxed *Ube3a* allele (*Ube3a*$^{FLOX/p+}$) (Figure S1). We first crossed *Ube3a*$^{FLOX/p+}$ mice to a *Gad2-Cre* line in which Cre is expressed by almost all inhibitory GABAergic neurons throughout the brain (Taniguchi et al., 2011). We immunohistochemically confirmed loss of UBE3A expression by GABAergic interneurons in adult *Ube3a*$^{FLOX/p+}$*::Gad2-Cre* mice, including parvalbumin-expressing subtypes in primary visual cortex (V1) (Figure 1A$_2$). The density of these interneuron subtypes in V1 was normal (Figure S2A), indicating that GABAergic *Ube3a* loss does not grossly disrupt GABAergic neuronal architecture in the neocortex. Moreover, GABAergic *Ube3a* loss in *Ube3a*$^{FLOX/p+}$*::Gad2-Cre* mice proved to be selective, as UBE3A co-staining with the L2–4 glutamatergic neuron marker, Cux1 (Nieto et al., 2004), was intact (Figure 1A$_1$ and 1A$_2$).

We then sought to determine if GABAergic neuron-specific loss of maternal *Ube3a* is sufficient to alter synaptic drive onto L2/3 pyramidal neurons, testing *Ube3a*$^{FLOX/p+}$*::Gad2-Cre* mice for the same spectrum of synaptic defects that we had previously observed in V1 of AS model mice (*Ube3a*$^{m-/p+}$) (Wallace et al., 2012). As expected, we found no difference in mEPSC amplitude or frequency onto L2/3 pyramidal neurons in *Ube3a*$^{FLOX/p+}$*::Gad2-Cre* compared to *Control* mice (Figure S2B). We also observed normal mIPSC amplitude and frequency in *Ube3a*$^{FLOX/p+}$*::Gad2-Cre* mice (Figure 1C), indicating that spontaneous GABAergic synaptic transmission remains intact following GABAergic neuron-specific loss of maternal *Ube3a*. This was unexpected, in view of previous evidence that decreased mIPSC frequency is a core GABAergic synaptic defect onto L2/3 pyramidal neurons in *Ube3a*$^{m-/p+}$ mice (Table 1; Wallace et al., 2012).

We were even more surprised to find that GABAergic *Ube3a* loss yields neither of two core deficits in electrically-evoked inhibition observed in *Ube3a*$^{m-/p+}$ mice: decreased evoked inhibitory postsynaptic current (eIPSC) amplitude or blunted recovery of GABAergic synaptic responses following high-frequency stimulation (Table 1). By stimulating (150 μm inferior to the recorded neuron) at a range of intensities, we revealed that eIPSC response amplitudes in *Ube3a*$^{FLOX/p+}$*::Gad2-Cre* mice are equivalent to *Control* (Figure 1D),

indicating that the strength of GABAergic inputs onto L2/3 pyramidal neurons develops normally following GABAergic *Ube3a* loss. To test the recovery of GABAergic synaptic transmission following high-frequency stimulation, we applied a train of 800 stimuli at 30 Hz to deplete reserves of GABAergic vesicles, followed immediately by 0.33 Hz stimulation to allow for recovery (Figure $1E_1$). We recorded eIPSC amplitudes from L2/3 pyramidal neurons during both phases of this experiment, to gauge rates of GABAergic synaptic depletion and recovery. Depletion of eIPSC amplitude in $Ube3a^{FLOX/p+}$*::Gad2-Cre* mice was equivalent to *Control* (Figure $1E_2$), as was recovery (Figure $1E_3$). Although eIPSC paired-pulse ratio in $Ube3a^{FLOX/p+}$*::Gad2-Cre* mice was subtly decreased when stimulating with a 100 ms inter-stimulus interval (ISI), eIPSC paired-pulse with 33 ms ISI was normal (Figure S2C). Thus, short-term plasticity at this synapse is largely intact following GABAergic *Ube3a* loss, particularly in response to the stimulation frequency we used to deplete GABAergic synapses (Figure 1E2).

Importantly, nervous system-wide deletion of $Ube3a^{FLOX/p+}$ ($Ube3a^{FLOX/p+}$*::Nestin-Cre*) produced a loss of *Ube3a* expression that was indistinguishable from *Ube3a* loss in $Ube3a^{m-/p+}$ mice (Figure S3); moreover, $Ube3a^{FLOX/p+}$*::Nestin-Cre* mice closely phenocopied L2/3 GABAergic synaptic defects in $Ube3a^{m-/p+}$ mice (Table 1 and Figure S4). $Ube3a^{FLOX}$ thus appears to be a viable conditional null allele, supporting the lack of phenotypic penetrance in $Ube3a^{FLOX/p+}$*::Gad2-Cre* mice as a genuine finding, rather than an artifact of residual *Ube3a* function following *Gad2-Cre*-mediated deletion. Collectively, these observations indicate that GABAergic *Ube3a* loss does not severely impair GABAergic synaptic drive onto L2/3 pyramidal neurons as results from *Ube3a* loss in all neurons (Table 1).

## Glutamatergic *Ube3a* Loss Impairs Electrically Evoked and Tonic GABAergic Inhibition onto L2/3 Pyramidal Neurons

To model glutamatergic *Ube3a* loss in a manner truly reciprocal to GABAergic *Ube3a* loss in $Ube3a^{FLOX/p+}$*::Gad2-Cre* mice, we crossed conditional *Ube3a* reinstatement mice ($Ube3a^{STOP/p+}$) to the same *Gad2-Cre* line. $Ube3a^{STOP/p+}$ mice constitute a conditional AS model in which expression of the maternal *Ube3a* allele is interrupted by targeted insertion of a floxed STOP cassette. Cre-mediated excision of the STOP cassette fully reinstates neuronal UBE3A expression in $Ube3a^{STOP/p+}$ mice (Silva-Santos et al., 2015). Hence, when we crossed $Ube3a^{STOP/p+}$ mice to *Gad2-Cre* mice ($Ube3a^{STOP/p+}$*::Gad2-Cre*), we observed UBE3A reinstatement that was specific to GABAergic interneurons in the neocortex, leaving neighboring Cux1-expressing glutamatergic neurons devoid of UBE3A expression in L2/3 neocortex (Figure 2A). Thus, $Ube3a^{STOP/p+}$*::Gad2-Cre* mice are an appropriate model of glutamatergic *Ube3a* loss.

To evaluate whether glutamatergic *Ube3a* loss in $Ube3a^{STOP/p+}$*::Gad2-Cre* mice could impair GABAergic synaptic drive onto L2/3 pyramidal neurons, we first needed to determine the extent to which $Ube3a^{STOP/p+}$ mice recapitulated key GABAergic synaptic defects. We found that $Ube3a^{STOP/p+}$ mice closely phenocopied $Ube3a^{m-/p+}$ and $Ube3a^{FLOX/p+}$*::Nestin-Cre* mice with respect to reduced eIPSC amplitude (Figure 2C) and blunted recovery from inhibitory synaptic depletion (Figure 2D). However, $Ube3a^{STOP/p+}$

mice failed to exhibit mIPSC amplitude or frequency deficits despite our experimentation with near-physiological as well as increased intracellular chloride levels (Figure S5B and S5C). It is possible that *Ube3a*$^{STOP}$ allele readthrough provided enough *Ube3a* expression, albeit very low (Silva-Santos et al., 2015), to selectively mitigate penetrance of the mIPSC deficit. Regardless of the underlying reason for this result, we were limited to evaluating only eIPSC amplitude and GABAergic synaptic recovery in *Ube3a*$^{STOP/p+}$*::Gad2-Cre* mice.

*Ube3a*$^{STOP/p+}$*::Gad2-Cre* mice proved to be statistically indistinguishable from *Ube3a*$^{STOP/p+}$ (but also *Control*) mice on measures of eIPSC amplitude (Figure 2C), providing a clue that glutamatergic *Ube3a* loss diminishes L2/3 pyramidal neuron responses to evoked GABAergic neurotransmission. Similar to *Ube3a*$^{STOP/p+}$ and *Control* mice, *Ube3a*$^{STOP/p+}$*::Gad2-Cre* mice showed no impairment on measures of mEPSCs, eIPSC paired-pulse ratios, or inhibitory synaptic depletion dynamics (Figure S5A, S5D, S5E$_1$, and S5E$_2$). In contrast, the blunted recovery from GABAergic synaptic depletion that we observed in *Ube3a*$^{STOP/p+}$ mice was completely absent in *Ube3a*$^{STOP/p+}$*::Gad2-Cre* mice (Figure 2D). This result demonstrates that glutamatergic *Ube3a* loss, just like GABAergic *Ube3a* loss (Figure 1E), fails to impair GABAergic synaptic recovery from high-frequency stimulation.

Selective manipulations of glutamatergic *Ube3a* expression in the neocortex should affect the penetrance of eIPSC amplitude deficits, assuming these deficits are secondary to an intrinsic loss of UBE3A function within L2/3 pyramidal neurons. We tested this assumption with several approaches. First, we crossed *Ube3a*$^{STOP/p+}$ mice to a NEX-*Cre* line (*Ube3a*$^{STOP/p+}$*::NEX-Cre*) in which *Ube3a* is selectively reinstated in glutamatergic neurons of the dorsal pallium, including Cux1-positive neurons of L2/3 neocortex (Figure 3A$_3$). eIPSC amplitudes in *Ube3a*$^{STOP/p+}$*::NEX-Cre* mice were similar to *Control* (Figure 3B and 3C), supporting that this deficit in *Ube3a*$^{STOP/p+}$ mice is driven by glutamatergic, not GABAergic, *Ube3a* loss in L2/3 neocortex, in agreement with our findings from *Ube3a*$^{FLOX/p+}$*::Gad2-Cre* mice (Figure 1D). To further demonstrate the neuron type-specificity of this phenotype, we probed *Ube3a*$^{FLOX/p+}$*::NEX-Cre* mice (Figure 3A$_4$), observing that neocortical glutamatergic *Ube3a* deletion was sufficient to yield the eIPSC deficit (Figure 3D and 3E). Finally, to test the cell autonomy of the effect, we intracerebroventricularly delivered low titers of Cre-expressing adeno-associated virus (AAV-Cre) to neonatal *Ube3a*$^{FLOX/p+}$ and *Ube3a*$^{m+/p+}$ control littermates (Figure S6A$_1$). This produced a sparse mosaic of virally-transduced neocortical neurons, including pyramidal neurons, which we identified by expression of a Cre-dependent tdTomato reporter. We observed a total loss of UBE3A expression in over 80% of tdTomato-positive neurons in *Ube3a*$^{FLOX/p+}$ mice by P12 (Figure S6A$_3$ and S6A$_4$). Conversely, almost all (>90%) tdTomato-positive neurons expressed UBE3A in *Ube3a*$^{m+/p+}$ littermates (Figure S6A$_2$ and S6A4). We measured eIPSC amplitude in mice prepared in this manner at ~P80, recording from tdTomato-positive L2/3 pyramidal neurons (*Ube3a*$^{FLOX/p+}$*::AAV-Cre or Ube3a*$^{m+/p+}$*::AAV-Cre*), as well as neighboring non-transduced L2/3 pyramidal neurons (*Ube3a*$^{FLOX/p+}$ *or Ube3a*$^{m+/p+}$) in V1 (Figure S6B$_1$). We observed reduced eIPSC amplitude in response to a range of stimulation intensities in *Ube3a*$^{FLOX/p+}$*::AAV-Cre* neurons compared to *Ube3a*$^{m+/p+}$*::AA V-Cre, Ube3a*$^{FLOX/p+}$, or *Ube3a*$^{m+/p+}$ neurons (Figure S6B$_2$

and S6B$_3$). We therefore conclude that diminished eIPSC amplitude onto L2/3 pyramidal neurons in AS mice is due to cell-autonomous consequences of *Ube3a* loss.

Intriguingly, deficits in eIPSC amplitude in *Ube3a*$^{FLOX/p+}$*::NEX-Cre* mice occurred in the absence of changes in either mIPSC amplitude or frequency (Figure 3F), indicating that synaptic GABA$_A$R function may be normal following glutamatergic *Ube3a* deletion in the dorsal forebrain. This apparent phenotypic discrepancy may be explained by deficits in extrasynaptic, delta subunit-containing GABA$_A$Rs (δ-GABA$_A$Rs), which might only be revealed in instances of GABA spillover to extrasynaptic regions (for example, following strong electrical stimulation) (Wei et al., 2003). Because δ-GABA$_A$Rs are the principal mediators of tonic inhibition onto pyramidal neurons in the neocortex (Brickley and Mody, 2012), we reasoned that glutamatergic *Ube3a* loss might selectively impair this mode of GABAergic transmission by L2/3 pyramidal neurons. To test this, we bath-applied a δ-GABA$_A$R-selective concentration of THIP (Gaboxadol) to stimulate extrasynaptic GABA$_A$Rs, followed by a saturating concentration of the competitive GABA$_A$R antagonist, Gabazine (SR95531) (Figure 3G$_1$). We recorded corresponding changes in holding current in L2/3 pyramidal neurons, finding that we could stimulate significantly less THIP/Gabazine-sensitive tonic current in *Ube3a*$^{FLOX/p+}$*::NEX-Cre* mice relative to *Control* (Figure 3G$_2$). This effect was not an artifact of decreased cell size, as capacitances between the two genotypes were equivalent (Control n = 30 cells, 64.06 ± 3 pF; *Ube3a*$^{FLOX/p+}$*::NEX-Cre* n = 21 cells, 68.33 ± 4.71 pF; p = 0.43). Together, these observations support that glutamatergic *Ube3a* loss cell-autonomously impairs tonic GABAergic tone onto L2/3 pyramidal neurons.

## GABAergic, but not Glutamatergic, *Ube3a* Loss Enhances Seizure Susceptibility

Converging lines of evidence implicate deficits in tonic inhibition in the pathogenesis of epilepsy. In particular, *GABRD* missense mutations that reduce δ-GABA$_A$R-mediated currents are associated with generalized epilepsy in humans (Dibbens et al., 2004), and *Gabrd*$^{-/-}$ mice are prone to seizures (Spigelman et al., 2002; Maguire et al., 2005). Therefore, we hypothesized that deficits owed to glutamatergic *Ube3a loss*, including impaired tonic δ-GABA$_A$R-mediated inhibition onto pyramidal neurons, would correlate with enhanced seizure susceptibility.

Latencies to seizure following an initial exposure to the putative GABA$_A$R antagonist, flurothyl, provide a reliable index of seizure threshold in naïve mice, and flurothyl seizures are highly penetrant regardless of genetic background (Krasowski, 2000; Kadiyala et al., 2014). We therefore used flurothyl to test seizure susceptibility in congenic C57BL/6 *Ube3a*$^{FLOX/p+}$*::NEX-Cre* mice (Figure 4A$_1$ and 4B). Surprisingly, we found that their latency to myoclonic and generalized seizure was similar to *Control* (Figure 4C). This finding indicates that decreased tonic GABAergic inhibition onto L2/3 pyramidal neurons does not confer vulnerability to seizures. Nor, in all likelihood, does any other physiological consequence of glutamatergic *Ube3a* loss in the dorsal telencephalon. In contrast, pan-cerebral GABAergic *Ube3a* loss on a congenic C57BL/6 background yielded a dramatic reduction in latency to myoclonus and generalized seizure, and even enhanced lethality to

repeated (once daily) exposures to flurothyl, as evinced by experiments in *Ube3a*$^{FLOX/p+}$*::Gad2-Cre* mice (Figure 4A$_2$ and 4D).

Notably, *NEX-Cre* does not mediate glutamatergic *Ube3a* deletion in ventral neuron populations, nor in the majority of dentate granule neurons (Figure 4A$_1$; Goebbels et al., 2006). Dentate granule neurons in particular receive an abundance of tonic GABAergic inhibition and are critical for gating temporal lobe excitability (Coulter and Carlson, 2007; Hsu, 2007; Pun et al., 2012), which might explain why *Ube3a*$^{FLOX/p+}$*::NEX-Cre* mice exhibit a normal response to flurothyl (Figure 4C). In contrast, *Ube3a*$^{STOP/p+}$*::Gad2-Cre* mice effectively model pan-cerebral glutamatergic *Ube3a* loss and thus provide a better model in which to fully evaluate the potential for glutamatergic *Ube3a* loss to enhance seizure susceptibility. As we maintain congenic129S2/SvPasCrl *Ube3a*$^{STOP/p+}$ mice, we turned to a sensory-evoked, audiogenic seizure induction paradigm that is suited to assessing seizure susceptibility on this genetic background (Figure 5A). Importantly, the audiogenic seizure paradigm has previously been used to demonstrate enhanced seizure susceptibility in AS mouse models on a 129 background, including *Ube3a*$^{m-/p+}$ and *Ube3a*$^{STOP/p+}$ mice (Jiang et al., 1998; van Woerden et al., 2007; Silva-Santos et al., 2015).

We confirmed that 129S2/SvPasCrl *Ube3a*$^{STOP/p+}$ mice are much more susceptible to audiogenic seizures than their *Control* littermates in terms of both frequency and severity (Figure 5B). *Ube3a*$^{STOP/p+}$*::Gad2-Cre* littermates, on the other hand, proved to be refractory to audiogenic seizure induction, similar to *Control* (Figure 5B). In contrast, consistent with our flurothyl-induced seizure results, we found that 129S2/SvPasCrl *Ube3a*$^{FLOX/p+}$*::Gad2-Cre* mice exhibit audiogenic seizures much more frequently than *Control* littermates and with a far greater likelihood of progressing from wild running to a severe, tonic-clonic episode (Figure 5C). Surprisingly, post-weaning lethality approached 15% in *Ube3a*$^{FLOX/p+}$*::Gad2-Cre* mice, and was associated with observations of spontaneous seizures (Figure 5D), whereas we observed no evidence of postnatal lethality associated with spontaneous seizures in *Ube3a*$^{STOP/p+}$ mice. Collectively, these findings provide compelling evidence that GABAergic, but not glutamatergic, *Ube3a* loss enhances seizure susceptibility. Notably, seizures due to GABAergic *Ube3a* loss alone are more severe than those observed in AS mice with loss of *Ube3a* in both GABAergic and glutamatergic neurons (Table 1).

## GABAergic, but not Glutamatergic, *Ube3a* Loss Mediates AS-like EEG Abnormalities

If GABAergic *Ube3a* loss drives seizure susceptibility in AS, then it might also underlie AS-like EEG abnormalities, including rhythmic, high-amplitude activity in the delta and theta bands (Thibert et al., 2013). To investigate this possibility, we recorded resting-state local field potentials (LFP, analogous to intracortical EEG (Buzsaki et al., 2012)) in awake head-fixed mice viewing a gray screen to which they were previously habituated (Figure 6A). We observed a strong trend toward total spectral power being increased in *Ube3a*$^{FLOX/p+}$*::Gad2-Cre* mice relative to *Control* (1–50 Hz power in $\mu V^2$: *Control* = 3915 ± 485.8; *Ube3a*$^{FLOX/p+}$*::Gad2-Cre* = 4292 ± 293.5; p = 0.07), primarily driven by enhancements in the delta band (Figure 6B). Increased power in other bands including theta (5–10 Hz power in $\mu V^2$: *Control* = 755 ± 101.2; *Ube3a*$^{FLOX/p+}$*::Gad2-Cre* = 873 ± 46.8; p = 0.3) and gamma (30–50 Hz power in $\mu V^2$: *Control* = 90 ± 9.8; *Ube3a*$^{FLOX/p+}$*::Gad2-Cre* = 101 ± 6; p = 0.37)

did not reach statistical significance. Total neocortical power was similarly elevated in *Ube3a*$^{STOP/p+}$ mice (Figure 6C), again largely through delta, with marginal power enhancement in other bands. However, LFP power in *Ube3a*$^{STOP/p+}$*::Gad2-Cre* mice, which model glutamatergic *Ube3a* loss, was normal (Figure 6C); total (1–50 Hz power in $\mu V^2$: *Control* = 3067 ± 252.7; *Ube3a*$^{STOP/p+}$ = 4255 ± 529.4; *Ube3a*$^{STOP/p+}$*::Gad2-Cre* = 2755 ± 391.5; p = 0.03), theta (5–10 Hz power in $\mu V^2$: *Control* = 733 ± 53.8; *Ube3a*$^{STOP/p+}$ = 879 ± 68.1; *Ube3a*$^{STOP/p+}$*::Gad2-Cre* = 647 ± 92.5; p = 0.11) and gamma (30–50 Hz power in $\mu V^2$: *Control* = 105 ± 10.7; *Ube3a*$^{STOP/p+}$ = 127 ± 13.4; *Ube3a*$^{STOP/p+}$*::Gad2-Cre* = 91 ± 13.3; p = 0.16) power was equivalent between *Control* and *Ube3a*$^{STOP/p+}$*::Gad2-Cre* mice. We therefore conclude that GABAergic, but not glutamatergic, *Ube3a* loss yields AS-like enhancements in EEG delta power (Table 1).

## GABAergic *Ube3a* Loss Phenocopies Presynaptic CCV Accumulations in AS Mice

We previously linked deficits in inhibitory synaptic recovery in *Ube3a*$^{m-/p+}$ mice to an aberrant accumulation of CCVs at GABAergic synapses (Wallace et al., 2012). This correlation suggests that maternal *Ube3a* loss may cause defective vesicle cycling, which fails to adequately restore presynaptic vesicle pools following bouts of high-frequency release (Cremona et al., 1999; Luthi et al., 2001; Milosevic et al., 2011). However, GABAergic synaptic depletion is normal in *Ube3a*$^{FLOX/p+}$*::Gad2-Cre* mice (Figure 1E), leading us to question whether GABAergic *Ube3a* loss would lead to aberrant presynaptic CCVs. First, we verified that pan-cerebral deletion of the maternal *Ube3a*$^{FLOX}$ allele results in the CCV phenotype, finding that CCVs were increased at dendritic and somatic GABAergic synapses in *Ube3a*$^{FLOX/p+}$*::Nestin-Cre* mice compared to *Control* (Figure S7A, S7B, and S7C). We also found that CCVs accumulate at glutamatergic synapses in these mice (Figure S7A and S7D), a departure from what we had previously observed in *Ube3a*$^{m-/p+}$ mice, where CCV increases at glutamatergic synapses did not reach statistical significance (Table 1). Next, we tested the effect of GABAergic *Ube3a* deletion on the CCV phenotype, comparing *Ube3a*$^{FLOX/p+}$*::Gad2-Cre* mice with littermate *Controls*. *Ube3a*$^{FLOX/p+}$*::Gad2-Cre* mice did in fact exhibit excessive CCVs at GABAergic presynaptic terminals that synapsed onto the dendrites (Figure 7A$_3$) and somata (Figure 7A$_4$) of glutamatergic neurons in L2/3. Furthermore, we observed excessive CCVs at asymmetric glutamatergic synapses made onto dendritic spines in L2/3 (Figure 7A$_5$). Other presynaptic measures including terminal area (Figure S8A$_1$, S8B$_1$, and S8C$_1$), mitochondrial area (Figure S8A$_2$, S8B$_2$, and S8C$_2$), and the density of synaptic vesicles (Figure S8A$_3$, S8B$_3$, and S8C$_3$) were largely normal. Thus, GABAergic *Ube3a* loss phenocopies the presynaptic CCV abnormalities in AS mice despite leaving recovery from GABAergic synaptic depletion intact (Figure 1E).

Excessive CCV accumulation also proved to be a feature of both GABAergic and glutamatergic L2/3 synapses in *Ube3a*$^{STOP/p+}$ mice (Figure 7B). To determine if glutamatergic *Ube3a* loss would affect presynaptic CCVs, we compared *Ube3a*$^{STOP/p+}$*::Gad2-Cre* mice to both *Ube3a*$^{STOP/p+}$ and *Control* littermates. We found that *Ube3a*$^{STOP/p+}$*::Gad2-Cre* and *Control* mice were statistically equivalent on measures of CCV density at GABAergic and glutamatergic L2/3 synapses (Figure 7B), indicating that glutamatergic *Ube3a* loss does not contribute to this phenotype in AS mice. Presynaptic

measures of terminal area, mitochondrial area, and synaptic vesicle density were similar across the three genotypic groups (Figure S8D–F). Importantly, glutamatergic CCV accumulations in *Ube3a*$^{STOP/p+}$ mice occurred in the absence of deficits in glutamatergic synaptic depletion (Figure S5E), providing yet another example of phenotypic dissociation between presynaptic CCVs and the capacity for recovery from synaptic depletion.

## DISCUSSION

This work constitutes the first investigation of neuron type-specific contributions to the pathogenesis of circuit hyperexcitability in AS. We show that GABAergic *Ube3a* deletion produces AS-like enhancements in EEG delta power, enhances seizure susceptibility and severity, and results in aberrant L2/3 presynaptic CCV accumulations. In contrast, glutamatergic *Ube3a* loss impairs the receipt of tonic GABAergic inhibition by L2/3 pyramidal neurons, but does not lead to EEG abnormalities or confer vulnerability to seizures.

Our present results demonstrate that GABAergic *Ube3a* loss leads to EEG abnormalities and seizures without producing any of the defects in GABAergic inhibition that we previously observed in L2/3 neocortex in AS mice, which lack *Ube3a* in nearly all neurons (Wallace et al., 2012). The immediate implication of this surprising finding is that defective GABAergic inhibition onto L2/3 pyramidal neurons is neither a cause nor a consequence of circuit hyperexcitability in AS mice. This is consistent with a recent study indicating that EEG abnormalities and seizures occur by P30 in AS mice (Mandel-Brehm et al., 2015), prior to the emergence of mIPSC and eIPSC deficits onto L2/3 pyramidal neurons (Wallace et al., 2012).

Intriguingly, GABAergic *Ube3a* deletion produces atypical accumulations of CCVs in presynaptic terminals (Figure 7A$_3$ and 7A$_4$), despite failing to yield deficits in GABAergic synaptic recovery following high-frequency stimulation. Increased presynaptic CCVs are a hallmark of deficient clathrin-mediated endocytosis (Cremona et al., 1999; Luthi et al., 2001; Milosevic et al., 2011), though they could also possibly reflect compensation for impairments in clathrin-independent modes of synaptic vesicle recycling (Daly et al., 2000). Regardless of the underlying cause, accumulations of clathrin-coated endocytic profiles in the synapse typically predict electrophysiological impairments in synaptic depletion and recovery, especially within GABAergic interneurons that display high-frequency firing (Cremona et al., 1999; Luthi et al., 2001; Hayashi et al., 2008). Our electrical stimulation parameters might not have been optimized to reveal deficiencies in synaptic vesicle recycling, perhaps explaining the dissociation between this phenotype and GABAergic presynaptic CCV accumulations. More puzzling is the fact that selective GABAergic *Ube3a* loss led to CCV accumulations at glutamatergic synapses (Figure 7A$_5$); unless *Ube3a* loss in GABAergic neurons triggers cell-nonautonomous defects in synaptic vesicle cycling, we would expect CCV phenotypes to be confined to GABAergic terminals. The parsimonious explanation is that CCV accumulations provide a readout of circuit hyperexcitability owed to GABAergic *Ube3a* loss, signaling the recent history of high-frequency activity at both GABAergic and glutamatergic presynaptic terminals. It remains to be elucidated how *Ube3a* loss impairs GABAergic synaptic recovery in AS mice, but our data implicate a mechanism

requiring loss of *Ube3a* in both glutamatergic and GABAergic neurons (Figure $1E_3$ and $2D_3$).

## Implications of Defective Tonic GABAergic Inhibition in AS Mice

Here we show that glutamatergic *Ube3a* loss impairs the receipt of tonic GABAergic inhibition by L2/3 pyramidal neurons in the absence of EEG abnormalities and seizures (Figure 3G, Figure 5B, and Figure 6C), indicating a lack of relevance to the pathogenesis of hyperexcitability in AS. Considering the apparent cell-autonomous nature of this defect, it is reasonable to speculate that tonic GABAergic tone onto GABAergic neurons is also diminished in AS. However, such a deficit is equally unlikely to factor in the pathogenesis of hyperexcitability; GABAergic neuron-specific deletion of δ-$GABA_A$Rs actually enhances phasic inhibition, thereby suppressing hippocampal network excitability and seizure susceptibility (Lee and Maguire, 2013). Nevertheless, decreases in tonic GABAergic neurotransmission have the potential to alter network dynamics throughout the brain (Brickley and Mody, 2012; Lee and Maguire, 2014), and may contribute to the manifestation of AS phenotypes besides epilepsy. For example, tonic inhibitory deficits onto cerebellar granule cells in AS mice are linked to impaired locomotion, which is amenable to rescue by the δ-$GABA_A$R superagonist THIP (Gaboxadol) (Egawa et al., 2012). It has since been shown that cerebellar deficits consequent to the loss of tonic GABAergic inhibition onto cerebellar granule cells are clearly dissociable from locomotor defects (Bruinsma et al., 2015), suggesting that any therapeutic benefit of THIP for gross motor dysfunction works through the enhancement of tonic GABAergic inhibition in extracerebellar circuits. Together with our present findings, these studies underscore the need for further preclinical elucidation of a complex relationship between deficits in tonic inhibition and AS-like phenotypes; such knowledge will be essential to inform future clinical trials of THIP administration in AS patients – especially with regard to the selection of appropriate clinical endpoints.

## Insights into Circuit-Level Consequences of GABAergic *Ube3a* Loss

What are the physiological mechanisms by which GABAergic *Ube3a* loss contributes to circuit imbalance? We previously found that neocortical fast-spiking interneurons receive normal excitatory synaptic drive and display appropriate intrinsic excitability in the absence of *Ube3a* (Wallace et al., 2012), and our present studies indicate that a loss of GABAergic inhibition onto L2/3 pyramidal neurons is not involved in mediating circuit hyperexcitability (Figures 1, 4, 5, 6, and 7). These findings highlight the importance of moving beyond the L2/3 neocortical microcircuit to elucidate the physiological consequences of GABAergic *Ube3a* loss. While this is a vast parameter space, potentially involving numerous GABAergic neuron populations, our EEG findings point to a major role for the thalamic reticular nucleus (TRN). GABAergic TRN neurons directly regulate the oscillatory activity of thalamocortical circuits and, when activated, are capable of mediating selective enhancements of neocortical EEG power in the delta band (Zhang et al., 2009; Lewis et al., 2015) – the same power band in which we observed the majority of EEG power enhancement following GABAergic *Ube3a* loss. Indeed, pathological synchrony of TRN neurons has been implicated in the generation of delta frequency spike-wave oscillations and atypical absence seizures (Steriade, 2005; Huguenard and McCormick, 2007), both of which

are commonly observed in AS (Vendrame et al., 2012; Thibert et al., 2013). High-amplitude theta rhythmicity (4–6 Hz) with spiking is another common background EEG abnormality in AS (Thibert et al., 2013). Although this theta abnormality is most prominent in occipital regions, it seems to disappear by adolescence (Laan et al., 1997), perhaps explaining why we did not record significant enhancements in theta power in adult *Ube3a*$^{STOP/p+}$ or *Ube3a*$^{FLOX/p+}$*::Gad2-Cre* mice despite recording from V1 (Figure 6). Future work in AS models should focus on factors known to affect TRN neuron excitability and synchrony – including relative levels of excitatory and inhibitory synaptic drive, the integrity of gap junctions (Proulx et al., 2006; Lee et al., 2014), the expression of T-type calcium channels (Tsakiridou et al., 1995; Zhang et al., 2009), and cholinergic input (McCormick and Prince, 1986; Sun et al., 2013). However, intracortical GABAergic mechanisms that underlie pathological spike-wave discharges also remain of interest, especially those that engage disinhibitory circuitry (Pi et al., 2013; Hall et al., 2015).

Numerous GABAergic circuits outside the thalamus and cortex could also contribute to the enhancements in seizure susceptibility that we observed following GABAergic *Ube3a* loss. This might even be expected, considering the variety of seizure types known to occur in individuals with AS (Galvan-Manso et al., 2005; Thibert et al., 2013). GABAergic circuits in the temporal lobe, hypothalamus, and striatum are all potentially of interest, but have yet to be formally investigated. We have also yet to explore the possibility that GABAergic *Ube3a* loss mediates AS-like phenotypes other than EEG abnormalities and seizures. Recent findings suggest that GABAergic *Mecp2* loss precipitates the majority of Rett syndrome-like phenotypes in mice (Chao et al., 2010; Ito-Ishida et al., 2015). Considering the high degree of phenotypic overlap between AS and Rett syndrome (Jedele, 2007; Tan et al., 2014), this might foreshadow a similarly broad penetrance of AS-like phenotypes following GABAergic *Ube3a* loss. On the other hand, there is clearly divergence in the developmental mechanisms underlying AS and Rett syndrome, as indicated by studies modeling the temporal requirements for *Ube3a* and *Mecp2* gene reinstatement therapy, respectively (Guy et al., 2007; Silva-Santos et al., 2015).

## Neuron Type-Specific Strategies for the Treatment of Circuit Hyperexcitability in AS

*Ube3a*$^{STOP/p+}$*::Gad2-Cre* mice dually serve to model the effects of glutamatergic *Ube3a* loss as well as the therapeutic value of GABAergic *Ube3a* reinstatement. The lack of EEG abnormalities, seizures, and associated CCV accumulations in this line (Figures 5, 6, and 7) demonstrates the promise that GABAergic neuron-specific treatments hold for the treatment of hyperexcitability phenotypes in AS. However, this promise has its limits. Modeling of pan-cellular *Ube3a* reinstatement in *Ube3a*$^{STOP/p+}$ mice predicts closure of a critical period for the amelioration of hyperexcitability phenotypes very early during postnatal development (Silva-Santos et al., 2015). Furthermore, GABAergic neuron-specific therapeutic approaches in AS are unlikely to involve the reinstatement of *UBE3A* expression. The only tractable target for the reinstatement of *UBE3A* expression in individuals with AS is the paternal *UBE3A* allele. Paternal *UBE3A* is intact, but epigenetically silenced *in cis* by a long non-coding RNA that includes a 3' *UBE3A–antisense* (*UBE3A–ATS*) sequence (Rougeulle et al., 1998; Martins-Taylor et al., 2014). Thus far, successful preclinical efforts to unsilence paternal *Ube3a* have depended directly (Meng et al., 2015) or indirectly (Huang et al., 2012)

on the downregulation of *Ube3a–ATS*, which appears to be uniformly expressed by glutamatergic and GABAergic neurons. Therefore, signaling pathways that functionally intersect with UBE3A are more likely to provide neuron type-specific targets for the development of AS therapeutics.

As a proof of concept, genetic normalization of calcium/calmodulin-dependent kinase type 2-α subunit (CaMKII-α) inhibitory hyperphosphorylation – a signaling deficit which decreases CaMKII enzymatic activity in $Ube3a^{m-/p+}$ mice (Weeber et al., 2003) – rescues seizure phenotypes (van Woerden et al., 2007). Moreover, genetic reduction of the immediate-early gene, *Arc* ($Arc^{+/-}$), whose expression UBE3A may regulate either transcriptionally or posttranslationally through ubiquitination (Greer et al., 2010; Kuhnle et al., 2013), normalizes EEG and abnormal responses to audiogenic stimuli in $Ube3a^{m-/p+}$ mice (Mandel-Brehm et al., 2015). *Arc* expression is preferentially induced in CaMKII-a-expressing neurons in response to convulsive seizures (Vazdarjanova et al., 2006), indicating that the restoration of circuit balance in $Ube3a^{m-/p+}::Arc^{+/-}$ mice may also be mediated by these cells. This poses a puzzle, however, considering our compelling evidence that GABAergic, but not glutamatergic, *Ube3a* loss drives the pathogenesis of hyperexcitability; in most brain regions including the cortex and hippocampus, CaMKII-a expression is restricted to glutamatergic neurons (Benson et al., 1992). An exception is the striatum in which CaMKII-α activity and *Arc* expression are readily induced within GABAergic spiny projection neurons in response to a variety of stimuli (Tan et al., 2000; Choe and Wang, 2002; Vazdarjanova et al., 2006; Anderson et al., 2008). GABAergic spiny projection neurons may thus be a nexus for seizure susceptibility or seizure resistance as mediated by loss or reinstatement of *Ube3a*, respectively. Alternatively, normalization of CaMKII-a and ARC function may work intrinsically through glutamatergic circuits to dampen their excitability and restore circuit balance, countering inhibitory deficits mediated by GABAergic *Ube3a* loss.

In summary, the present data compel us to revisit, reevaluate, and refine our previous hypotheses regarding the pathogenesis of circuit hyperexcitability in AS. We now appreciate that GABAergic *UBE3A* loss is likely to be the principal pathogenic factor underlying circuit hyperexcitability in the disorder; accordingly, the restoration of GABAergic neuronal function represents the most direct therapeutic strategy for the prevention or reversal of EEG abnormalities and seizures, provided the intervention occurs sufficiently early in development. This conceptual advance should help to focus future studies of the molecular mechanisms working both upstream and downstream of UBE3A within GABAergic neurons, perhaps yielding novel, actionable therapeutic targets.

## EXPERIMENTAL PROCEDURES

See Supplemental Experimental Procedures for experimental details relating to mouse lines, AAV-Cre injections, electrophysiology, flurothyl-induced seizure assays, audiogenic seizure assays, qRT-PCR, Western blotting, immunohistochemistry, and statistical analyses.

## Animals

We raised all mice on a 12:12 lightdark cycle with ad libitum access to food and water. We used both male and female littermates at equivalent genotypic ratios and in strict compliance with animal protocols approved by the Institutional Animal Care and Use Committees of the University of North Carolina at Chapel Hill.

## Electrophysiology

**Whole-cell voltage-clamp recordings—**We placed coronal slices containing V1 (see Supplemental Experimental Procedures) in a submersion chamber maintained at 30° C and perfused at 2 mL/min with oxygenated ACSF (in mM; 124 NaCl, 3 KCl, 1.25 $NaH_2PO_4$, 26 $NaHCO_3$, 1 $MgCl_2$, 2 $CaCl_2$, and 20 dextrose). We pulled patch pipettes from thick-walled borosilicate glass using a P2000 laser puller (Sutter Instruments, Novato, CA). Open tip resistances were between 2–5 MΩ when pipettes were filled with the internal solution containing (in mM): 100 $CsCH_3SO_3$, 15 CsCl, 2.5 $MgCl_2$, 5 QX-314-Cl, 5 tetra-Cs-BAPTA, 10 HEPES, 4 Mg-ATP, 0.3 Na-GTP, and 0.025 Alexa-594, with pH adjusted to 7.25 and osmolarity adjusted to ~295 mOsm with sucrose.

We visually targeted L2/3 pyramidal neurons for recording using an Axio Examiner microscope (Zeiss, Germany) equipped with infrared differential interference contrast and epifluorescence optics. For successfully patched neurons, we achieved pipette seal resistances > 1 GΩ, minimizing pipette capacitive transients prior to breakthrough. We performed voltage-clamp recordings in the whole-cell configuration using a Multiclamp 700B amplifier (Molecular Devices, Sunnyvale, CA) with 10 kHz digitization and a 2 kHz low-pass Bessel filter. We acquired and analyzed data using pCLAMP 10 software (Molecular Devices, RRID:SCR_011323). We monitored changes in series and input resistance throughout each experiment by giving test step of −5 mV every 30 s and measuring the resultant amplitude of the capacitive current. We discarded neurons if series resistance surpassed 25 MΩ or if series resistance or input resistance changed by >25% during the course of an experiment. We confirmed L2/3 pyramidal neuronal identity by analyzing characteristic membrane properties (Supplemental Table 1) and the presence of dendritic spines and prominent apical dendrites visualized with Alexa-594 dye.

**In vivo local field potential (LFP) recordings—**We backcrossed mice used for LFP and audiogenic seizure experiments (see Supplemental Experimental Procedures) 6–7 generations onto the 129S2/SvPasCrl background, which is permissive for hyperexcitability phenotypes. For surgeries, we anesthetized adult mice (P75–118 on day 1 of recording) via intraperitoneal injections of ketamine (40 mg/kg) and xylazine (10 mg/kg), with 0.25% bupivacaine injected under the scalp for local analgesia. We then bilaterally implanted tungsten microelectrodes (FHC, Bowdoin, ME) in layer 4 of V1 (3.2–3.3 mm lateral to Lambda, 0.47 mm depth) and placed a silver wire in prefrontal cortex as a reference electrode. In order to enable head fixation during recordings, we attached a steel headpost to the skull anterior to bregma. We used dental cement to secure all elements in place and create a protective head cap.

We allowed mice to recover for at least 2 days following surgery before habituating them to the recording apparatus over 2 consecutive days. We acquired LFP data over the next 3 consecutive days. We head-fixed mice during all recording sessions (both habituation and LFP), orienting them towards a full-field gray screen for 15 minutes in a dark, quiet environment. We amplified LFP recordings 1000x using single-channel amplifiers (Grass Technologies, Warwick, RI) with 0.1 Hz low-pass and 100 Hz high-pass filtration preceding acquisition and digitization at 4 kHz using Spike2 software (CED Ltd., Cambridge, UK, RRID:SCR_000903). We analyzed spectral power using a fast Fourier transform resulting in bin sizes of 0.5 Hz. Prior to analysis, we manually excluded rarely occurring electrical artifacts corresponding to mouse movement. For each animal, we averaged power spectra from both hemispheres across all three days of recording.

### Statistics

We performed all experiments and analyses blind to genotype. We performed all statistical analyses using GraphPad Prism 6 software (GraphPad Software Inc., La Jolla, CA, RRID:SCR_002798).

## Supplementary Material

Refer to Web version on PubMed Central for supplementary material.

## Acknowledgments

We thank Rylan Larsen and Janet Berrios for critical readings of the manuscript, Hyojin Kim for maintaining animal colonies, Kristen Phend for histological support, Dale Cowley and George Altshuller at the UNC Animal Models Core, William D. Snider for providing AAV-Cre virus, and Klaus-Armin Nave for providing *NEX-Cre* mice. This work was supported by NRSA fellowships 5F32NS077686 (to M.J.) and 1F31NS077847 (to M.W.), an NRSA institutional postdoctoral training grant T32-HD40127 (to M.S.), the Angelman Syndrome Foundation's Joseph E. Wagstaff fellowship (to I.K.), Angelman Syndrome Foundation grants (to Y.E. and B.P.), Simons Foundation SFARI Awards 274426 (to B.P.) and 275234 (to Y.E.), a Netherlands Organization for Scientific Research grant-ZonNMW (to Y.E.), a Hersenstichting grant (to G.v.W.), NIMH 5RO1MHO93372 (to M.Z. and B.P.), NINDS 5RO1NS039444 (to R.W.), and NINDS 1RO1NS085093 (to B.P.). Confocal imaging was supported by NINDS Center Grant P30 NS045892 and NICHD Center Grant P30 HD03110. NIH grants to Velocigene at Regeneron Inc. (U01HG004085), the CSD Consortium (U01HG004080), and the KOMP Repository at UC Davis and CHORI (U42RR024244) funded the generation, curation, and distribution of the targeting vector used to produce $Ube3a^{FLOX}$ mice.

## REFERENCES

Anderson SM, Famous KR, Sadri-Vakili G, Kumaresan V, Schmidt HD, Bass CE, Terwilliger EF, Cha JH, Pierce RC. CaMKII: a biochemical bridge linking accumbens dopamine and glutamate systems in cocaine seeking. Nat Neurosci. 2008; 11:344–353. [PubMed: 18278040]

Benson DL, Isackson PJ, Gall CM, Jones EG. Contrasting patterns in the localization of glutamic acid decarboxylase and Ca2+/calmodulin protein kinase gene expression in the rat central nervous system. Neuroscience. 1992; 46:825–849. [PubMed: 1311814]

Brickley SG, Mody I. Extrasynaptic GABA(A) receptors: their function in the CNS and implications for disease. Neuron. 2012; 73:23–34. [PubMed: 22243744]

Bruinsma CF, Schonewille M, Gao Z, Aronica EM, Judson MC, Philpot BD, Hoebeek FE, van Woerden GM, De Zeeuw CI, Elgersma Y. Dissociation of locomotor and cerebellar deficits in a murine Angelman syndrome model. J Clin Invest. 2015; 125:4305–4315. [PubMed: 26485287]

Buzsaki G, Anastassiou CA, Koch C. The origin of extracellular fields and currents--EEG, ECoG, LFP and spikes. Nat Rev Neurosci. 2012; 13:407–420. [PubMed: 22595786]

Chao HT, Chen H, Samaco RC, Xue M, Chahrour M, Yoo J, Neul JL, Gong S, Lu HC, Heintz N, et al. Dysfunction in GABA signalling mediates autism-like stereotypies and Rett syndrome phenotypes. Nature. 2010; 468:263–269. [PubMed: 21068835]

Choe ES, Wang JQ. CaMKII regulates amphetamine-induced ERK1/2 phosphorylation in striatal neurons. Neuroreport. 2002; 13:1013–1016. [PubMed: 12060798]

Cooper EM, Hudson AW, Amos J, Wagstaff J, Howley PM. Biochemical analysis of Angelman syndrome-associated mutations in the E3 ubiquitin ligase E6-associated protein. J Biol Chem. 2004; 279:41208–41217. [PubMed: 15263005]

Coulter DA, Carlson GC. Functional regulation of the dentate gyrus by GABA-mediated inhibition. Prog Brain Res. 2007; 163:235–243. [PubMed: 17765722]

Cremona O, Di Paolo G, Wenk MR, Luthi A, Kim WT, Takei K, Daniell L, Nemoto Y, Shears SB, Flavell RA, et al. Essential role of phosphoinositide metabolism in synaptic vesicle recycling. Cell. 1999; 99:179–188. [PubMed: 10535736]

Daly C, Sugimori M, Moreira JE, Ziff EB, Llinas R. Synaptophysin regulates clathrin-independent endocytosis of synaptic vesicles. Proc Natl Acad Sci U S A. 2000; 97:6120–6125. [PubMed: 10823955]

Dibbens LM, Feng HJ, Richards MC, Harkin LA, Hodgson BL, Scott D, Jenkins M, Petrou S, Sutherland GR, Scheffer IE, et al. GABRD encoding a protein for extra- or peri-synaptic GABAA receptors is a susceptibility locus for generalized epilepsies. Hum Mol Genet. 2004; 13:1315–1319. [PubMed: 15115768]

Egawa K, Kitagawa K, Inoue K, Takayama M, Takayama C, Saitoh S, Kishino T, Kitagawa M, Fukuda A. Decreased tonic inhibition in cerebellar granule cells causes motor dysfunction in a mouse model of Angelman syndrome. Sci Transl Med. 2012; 4:163ra157.

Galvan-Manso M, Campistol J, Conill J, Sanmarti FX. Analysis of the characteristics of epilepsy in 37 patients with the molecular diagnosis of Angelman syndrome. Epileptic Disord. 2005; 7:19–25. [PubMed: 15741136]

Goebbels S, Bormuth I, Bode U, Hermanson O, Schwab MH, Nave KA. Genetic targeting of principal neurons in neocortex and hippocampus of NEX-Cre mice. Genesis. 2006; 44:611–621. [PubMed: 17146780]

Greer PL, Hanayama R, Bloodgood BL, Mardinly AR, Lipton DM, Flavell SW, Kim TK, Griffith EC, Waldon Z, Maehr R, et al. The Angelman Syndrome protein Ube3A regulates synapse development by ubiquitinating arc. Cell. 2010; 140:704–716. [PubMed: 20211139]

Guy J, Gan J, Selfridge J, Cobb S, Bird A. Reversal of neurological defects in a mouse model of Rett syndrome. science. 2007; 315:1143–1147. [PubMed: 17289941]

Hall S, Hunt M, Simon A, Cunnington LG, Carracedo LM, Schofield IS, Forsyth R, Traub RD, Whittington MA. Unbalanced Peptidergic Inhibition in Superficial Neocortex Underlies Spike and Wave Seizure Activity. J Neurosci. 2015; 35:9302–9314. [PubMed: 26109655]

Hayashi M, Raimondi A, O'Toole E, Paradise S, Collesi C, Cremona O, Ferguson SM, De Camilli P. Cell- and stimulus-dependent heterogeneity of synaptic vesicle endocytic recycling mechanisms revealed by studies of dynamin 1-null neurons. Proc Natl Acad Sci U S A. 2008; 105:2175–2180. [PubMed: 18250322]

Hsu D. The dentate gyrus as a filter or gate: a look back and a look ahead. Prog Brain Res. 2007; 163:601–613. [PubMed: 17765740]

Huang HS, Allen JA, Mabb AM, King IF, Miriyala J, Taylor-Blake B, Sciaky N, Dutton JW Jr, Lee HM, Chen X, et al. Topoisomerase inhibitors unsilence the dormant allele of Ube3a in neurons. Nature. 2012; 481:185–189.

Huguenard JR, McCormick DA. Thalamic synchrony and dynamic regulation of global forebrain oscillations. Trends Neurosci. 2007; 30:350–356. [PubMed: 17544519]

Ito-Ishida A, Ure K, Chen H, Swann JW, Zoghbi HY. Loss of MeCP2 in Parvalbumin-and Somatostatin-Expressing Neurons in Mice Leads to Distinct Rett Syndromelike Phenotypes. Neuron. 2015; 88:651–658. [PubMed: 26590342]

Jedele KB. The overlapping spectrum of rett and angelman syndromes: a clinical review. Semin Pediatr Neurol. 2007; 14:108–117. [PubMed: 17980307]

Jiang YH, Armstrong D, Albrecht U, Atkins CM, Noebels JL, Eichele G, Sweatt JD, Beaudet AL. Mutation of the Angelman ubiquitin ligase in mice causes increased cytoplasmic p53 and deficits of contextual learning and long-term potentiation. Neuron. 1998; 21:799–811. [PubMed: 9808466]

Judson MC, Sosa-Pagan JO, Del Cid WA, Han JE, Philpot BD. Allelic specificity of Ube3a expression in the mouse brain during postnatal development. J Comp Neurol. 2014; 522:1874–1896. [PubMed: 24254964]

Kadiyala SB, Papandrea D, Herron BJ, Ferland RJ. Segregation of seizure traits in C57 black mouse substrains using the repeated-flurothyl model. PLoS One. 2014; 9:e90506. [PubMed: 24594686]

Kishino T, Lalande M, Wagstaff J. UBE3A/E6-AP mutations cause Angelman syndrome. Nat Genet. 1997; 15:70–73. [PubMed: 8988171]

Krasowski MD. Differential modulatory actions of the volatile convulsant flurothyl and its anesthetic isomer at inhibitory ligand-gated ion channels. Neuropharmacology. 2000; 39:1168–1183. [PubMed: 10760360]

Kuhnle S, Mothes B, Matentzoglu K, Scheffner M. Role of the ubiquitin ligase E6AP/UBE3A in controlling levels of the synaptic protein Arc. Proc Natl Acad Sci U S A. 2013; 110:8888–8893. [PubMed: 23671107]

Laan LA, Renier WO, Arts WF, Buntinx IM, vd Burgt IJ, Stroink H, Beuten J, Zwinderman KH, van Dijk JG, Brouwer OF. Evolution of epilepsy and EEG findings in Angelman syndrome. Epilepsia. 1997; 38:195–199. [PubMed: 9048672]

Lee SC, Patrick SL, Richardson KA, Connors BW. Two functionally distinct networks of gap junction-coupled inhibitory neurons in the thalamic reticular nucleus. J Neurosci. 2014; 34:13170–13182. [PubMed: 25253862]

Lee V, Maguire J. Impact of inhibitory constraint of interneurons on neuronal excitability. J Neurophysiol. 2013; 110:2520–2535. [PubMed: 24027099]

Lee V, Maguire J. The impact of tonic GABAA receptor-mediated inhibition on neuronal excitability varies across brain region and cell type. Front Neural Circuits. 2014; 8:3. [PubMed: 24550784]

Lewis LD, Voigts J, Flores FJ, Schmitt LI, Wilson MA, Halassa MM, Brown EN. Thalamic reticular nucleus induces fast and local modulation of arousal state. Elife. 2015:4.

Luthi A, Di Paolo G, Cremona O, Daniell L, De Camilli P, McCormick DA. Synaptojanin 1 contributes to maintaining the stability of GABAergic transmission in primary cultures of cortical neurons. J Neurosci. 2001; 21:9101–9111. [PubMed: 11717343]

Mabb AM, Ehlers MD. Ubiquitination in postsynaptic function and plasticity. Annu Rev Cell Dev Biol. 2010; 26:179–210. [PubMed: 20604708]

Mabb AM, Judson MC, Zylka MJ, Philpot BD. Angelman syndrome: insights into genomic imprinting and neurodevelopmental phenotypes. Trends Neurosci. 2011; 34:293–303. [PubMed: 21592595]

Maguire JL, Stell BM, Rafizadeh M, Mody I. Ovarian cycle-linked changes in GABA(A) receptors mediating tonic inhibition alter seizure susceptibility and anxiety. Nat Neurosci. 2005; 8:797–804. [PubMed: 15895085]

Mandel-Brehm C, Salogiannis J, Dhamne SC, Rotenberg A, Greenberg ME. Seizure-like activity in a juvenile Angelman syndrome mouse model is attenuated by reducing Arc expression. Proc Natl Acad Sci U S A. 2015; 112:5129–5134. [PubMed: 25848016]

Martins-Taylor K, Hsiao JS, Chen PF, Glatt-Deeley H, De Smith AJ, Blakemore AI, Lalande M, Chamberlain SJ. Imprinted expression of UBE3A in non-neuronal cells from a Prader-Willi syndrome patient with an atypical deletion. Hum Mol Genet. 2014; 23:2364–2373. [PubMed: 24363065]

Matsuura T, Sutcliffe JS, Fang P, Galjaard RJ, Jiang YH, Benton CS, Rommens JM, Beaudet AL. De novo truncating mutations in E6-AP ubiquitin-protein ligase gene (UBE3A) in Angelman syndrome. Nat Genet. 1997; 15:74–77. [PubMed: 8988172]

McCormick DA, Prince DA. Acetylcholine induces burst firing in thalamic reticular neurones by activating a potassium conductance. Nature. 1986; 319:402–405. [PubMed: 2418361]

Meng L, Ward AJ, Chun S, Bennett CF, Beaudet AL, Rigo F. Towards a therapy for Angelman syndrome by targeting a long non-coding RNA. Nature. 2015; 518:409–412. [PubMed: 25470045]

Milosevic I, Giovedi S, Lou X, Raimondi A, Collesi C, Shen H, Paradise S, O'Toole E, Ferguson S, Cremona O, et al. Recruitment of endophilin to clathrin-coated pit necks is required for efficient vesicle uncoating after fission. Neuron. 2011; 72:587–601. [PubMed: 22099461]

Nieto M, Monuki ES, Tang H, Imitola J, Haubst N, Khoury SJ, Cunningham J, Gotz M, Walsh CA. Expression of Cux-1 and Cux-2 in the subventricular zone and upper layers II-IV of the cerebral cortex. J Comp Neurol. 2004; 479:168–180. [PubMed: 15452856]

Pi HJ, Hangya B, Kvitsiani D, Sanders JI, Huang ZJ, Kepecs A. Cortical interneurons that specialize in disinhibitory control. Nature. 2013; 503:521–524. [PubMed: 24097352]

Proulx E, Leshchenko Y, Kokarovtseva L, Khokhotva V, El-Beheiry M, Snead OC 3rd, Perez Velazquez JL. Functional contribution of specific brain areas to absence seizures: role of thalamic gap-junctional coupling. Eur J Neurosci. 2006; 23:489–496. [PubMed: 16420455]

Pun RY, Rolle IJ, Lasarge CL, Hosford BE, Rosen JM, Uhl JD, Schmeltzer SN, Faulkner C, Bronson SL, Murphy BL, et al. Excessive activation of mTOR in postnatally generated granule cells is sufficient to cause epilepsy. Neuron. 2012; 75:1022–1034. [PubMed: 22998871]

Rotin D, Kumar S. Physiological functions of the HECT family of ubiquitin ligases. Nat Rev Mol Cell Biol. 2009; 10:398–409. [PubMed: 19436320]

Rougeulle C, Cardoso C, Fontes M, Colleaux L, Lalande M. An imprinted antisense RNA overlaps UBE3A and a second maternally expressed transcript. Nat Genet. 1998; 19:15–16. [PubMed: 9590281]

Rougeulle C, Glatt H, Lalande M. The Angelman syndrome candidate gene, UBE3A/E6-AP, is imprinted in brain. Nat Genet. 1997; 17:14–15. [PubMed: 9288088]

Silva-Santos S, van Woerden GM, Bruinsma CF, Mientjes E, Jolfaei MA, Distel B, Kushner SA, Elgersma Y. Ube3a reinstatement identifies distinct developmental windows in a murine Angelman syndrome model. J Clin Invest. 2015; 125:2069–2076. [PubMed: 25866966]

Spigelman I, Li Z, Banerjee PK, Mihalek RM, Homanics GE, Olsen RW. Behavior and physiology of mice lacking the GABAA-receptor delta subunit. Epilepsia. 2002; 5(43 Suppl):3–8. [PubMed: 12121286]

Steriade M. Sleep, epilepsy and thalamic reticular inhibitory neurons. Trends Neurosci. 2005; 28:317–324. [PubMed: 15927688]

Sun YG, Pita-Almenar JD, Wu CS, Renger JJ, Uebele VN, Lu HC, Beierlein M. Biphasic cholinergic synaptic transmission controls action potential activity in thalamic reticular nucleus neurons. J Neurosci. 2013; 33:2048–2059. [PubMed: 23365242]

Sutcliffe JS, Jiang YH, Galijaard RJ, Matsuura T, Fang P, Kubota T, Christian SL, Bressler J, Cattanach B, Ledbetter DH, et al. The E6-Ap ubiquitin-protein ligase (UBE3A) gene is localized within a narrowed Angelman syndrome critical region. Genome Res. 1997; 7:368–377. [PubMed: 9110176]

Tan A, Moratalla R, Lyford GL, Worley P, Graybiel AM. The activity-regulated cytoskeletal-associated protein arc is expressed in different striosome-matrix patterns following exposure to amphetamine and cocaine. J Neurochem. 2000; 74:2074–2078. [PubMed: 10800951]

Tan WH, Bird LM, Thibert RL, Williams CA. If not Angelman, what is it? A review of Angelman-like syndromes. Am J Med Genet A . 2014; 164A:975–992. [PubMed: 24779060]

Taniguchi H, He M, Wu P, Kim S, Paik R, Sugino K, Kvitsiani D, Fu Y, Lu J, Lin Y, et al. A resource of Cre driver lines for genetic targeting of GABAergic neurons in cerebral cortex. Neuron. 2011; 71:995–1013. [PubMed: 21943598]

Thibert RL, Larson AM, Hsieh DT, Raby AR, Thiele EA. Neurologic manifestations of Angelman syndrome. Pediatr Neurol. 2013; 48:271–279. [PubMed: 23498559]

Tsakiridou E, Bertollini L, de Curtis M, Avanzini G, Pape HC. Selective increase in T-type calcium conductance of reticular thalamic neurons in a rat model of absence epilepsy. J Neurosci. 1995; 15:3110–3117. [PubMed: 7722649]

van Woerden GM, Harris KD, Hojjati MR, Gustin RM, Qiu S, de Avila Freire R, Jiang YH, Elgersma Y, Weeber EJ. Rescue of neurological deficits in a mouse model for Angelman syndrome by reduction of alphaCaMKII inhibitory phosphorylation. Nat Neurosci. 2007; 10:280–282. [PubMed: 17259980]

Vazdarjanova A, Ramirez-Amaya V, Insel N, Plummer TK, Rosi S, Chowdhury S, Mikhael D, Worley PF, Guzowski JF, Barnes CA. Spatial exploration induces ARC, a plasticity-related immediate-early gene, only in calcium/calmodulin-dependent protein kinase II-positive principal excitatory and inhibitory neurons of the rat forebrain. J Comp Neurol. 2006; 498:317–329. [PubMed: 16871537]

Vendrame M, Loddenkemper T, Zarowski M, Gregas M, Shuhaiber H, Sarco DP, Morales A, Nespeca M, Sharpe C, Haas K, et al. Analysis of EEG patterns and genotypes in patients with Angelman syndrome. Epilepsy Behav. 2012; 23:261–265. [PubMed: 22341959]

Wallace ML, Burette AC, Weinberg RJ, Philpot BD. Maternal loss of Ube3a produces an excitatory/inhibitory imbalance through neuron type-specific synaptic defects. Neuron. 2012; 74:793–800. [PubMed: 22681684]

Weeber EJ, Jiang YH, Elgersma Y, Varga AW, Carrasquillo Y, Brown SE, Christian JM, Mirnikjoo B, Silva A, Beaudet AL, et al. Derangements of hippocampal calcium/calmodulin-dependent protein kinase II in a mouse model for Angelman mental retardation syndrome. J Neurosci. 2003; 23:2634–2644. [PubMed: 12684449]

Wei W, Zhang N, Peng Z, Houser CR, Mody I. Perisynaptic localization of delta subunit-containing GABA(A) receptors and their activation by GABA spillover in the mouse dentate gyrus. J Neurosci. 2003; 23:10650–10661. [PubMed: 14627650]

Williams CA, Beaudet AL, Clayton-Smith J, Knoll JH, Kyllerman M, Laan LA, Magenis RE, Moncla A, Schinzel AA, Summers JA, et al. Angelman syndrome 2005: updated consensus for diagnostic criteria. Am J Med Genet A. 2006; 140:413–418. [PubMed: 16470747]

Yamasaki K, Joh K, Ohta T, Masuzaki H, Ishimaru T, Mukai T, Niikawa N, Ogawa M, Wagstaff J, Kishino T. Neurons but not glial cells show reciprocal imprinting of sense and antisense transcripts of Ube3a. Hum Mol Genet. 2003; 12:837–847. [PubMed: 12668607]

Zhang Y, Llinas RR, Lisman JE. Inhibition of NMDARs in the Nucleus Reticularis of the Thalamus Produces Delta Frequency Bursting. Front Neural Circuits. 2009; 3:20. [PubMed: 20057928]

## HIGHLIGHTS

- Glutamatergic *Ube3a* loss decreases tonic inhibition onto L2/3 pyramidal neurons.
- GABAergic *Ube3a* loss does not compromise inhibition onto L2/3 pyramidal neurons.
- GABAergic, not glutamatergic, *Ube3a* loss causes EEG abnormalities and seizures.
- L2/3 GABAergic defects in AS mice neither cause, nor are caused by, seizures.

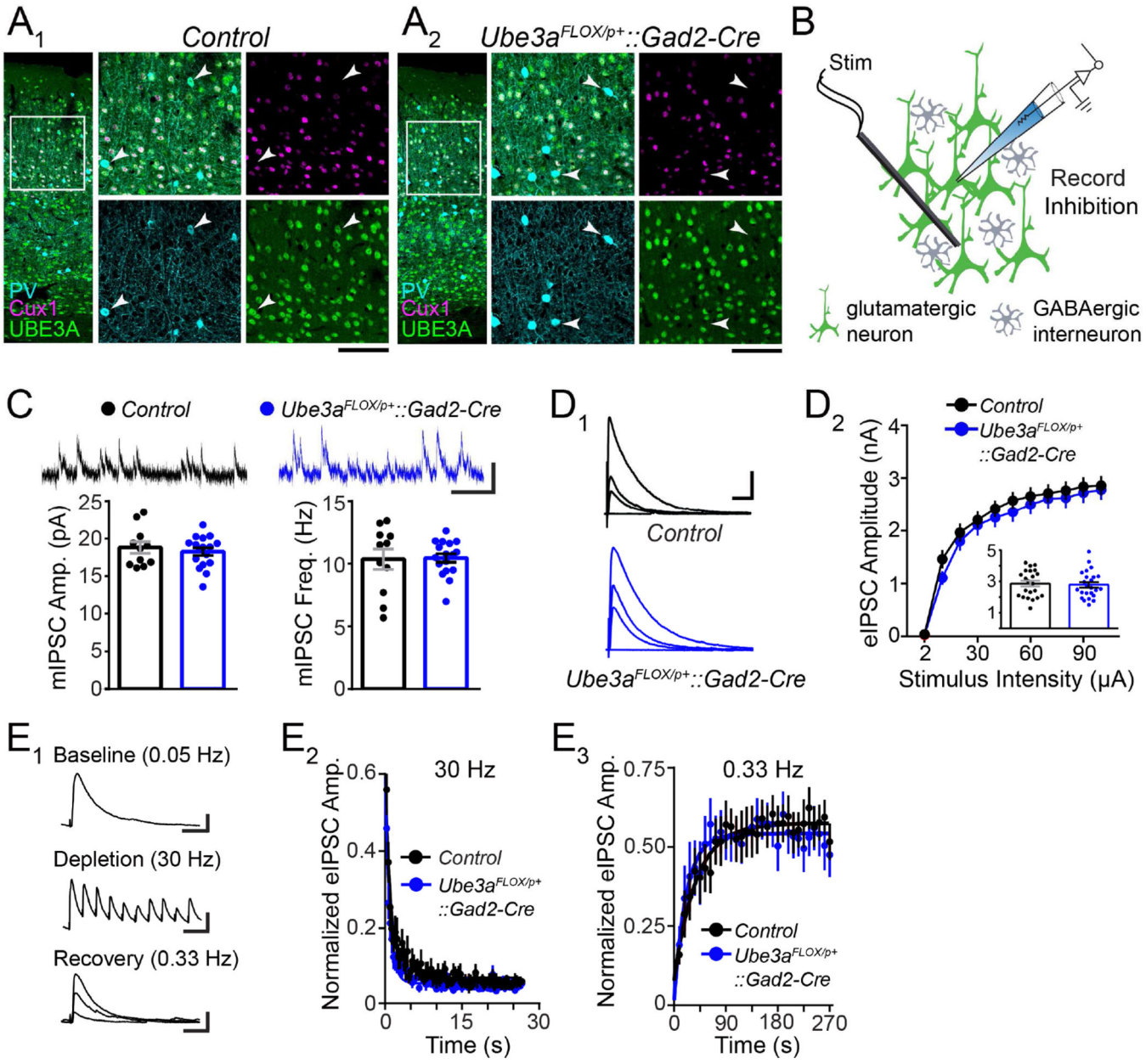


**Figure 1. GABAergic *Ube3a* loss does not compromise synaptic inhibition onto L2/3 pyramidal neurons**

(**A**) Immunostaining of parvalbumin (PV), Cux1, and UBE3A in V1 of ~P80 *Control* ($A_1$) and *Ube3a*$^{FLOX/p+}$*::Gad2-Cre* ($A_2$) mice. Arrowheads indicate PV-positive interneurons lacking UBE3A (scale bar = 145 μm or 75 μm for zoom-ins). (**B**) Schematic for recording synaptic inhibition onto L2/3 pyramidal neurons in V1 of ~P80 *Ube3a*$^{FLOX/p+}$*::Gad2-Cre* mice (green shading indicates presence of UBE3A). (**C**) Sample recordings (scale bar = 20 pA, 200 ms) and quantification of mIPSC amplitude and frequency (*Control* n = 11 cells; *Ube3a*$^{FLOX/p+}$*::Gad2-Cre* n = 17 cells). (**D**) Sample recordings of eIPSCs ($D_1$) at stimulation intensities of 2, 10, 30, and 100 μA (scale bar = 1 nA, 40 ms). ($D_2$) Quantification of eIPSCs. Inset depicts response amplitudes to 100 μ*A* stimulation (*Control* n = 22 cells;

*Ube3a*$^{FLOX/p+}$*::Gad2-Cre* n = 24 cells). (**E**) Sample recordings ($E_1$) depicting each phase of an inhibitory synaptic depletion and recovery experiment (scale bars: baseline = 200 pA, 20 ms; depletion = 200 pA, 70 ms; recovery = 200 pA, 20 ms). ($E_2$) Average depletion phase showing eIPSC amplitude normalized to baseline during 800 stimuli at 30 Hz. Each point (80 plotted per genotype) represents 10 consecutive responses that were collapsed and averaged per cell. ($E_3$) Average recovery phase showing eIPSC amplitude normalized to baseline during 90 stimuli at 0.33 Hz. Each point (30 plotted per genotype) represents 3 consecutive responses that were collapsed and averaged per cell. Average depletion and recovery responses for each genotype were fit with a monophasic exponential (*Control* n = 11 cells; *Ube3a*$^{FLOX/p+}$*::Gad2-Cre* n = 9 cells). Data represent mean ± SEM.

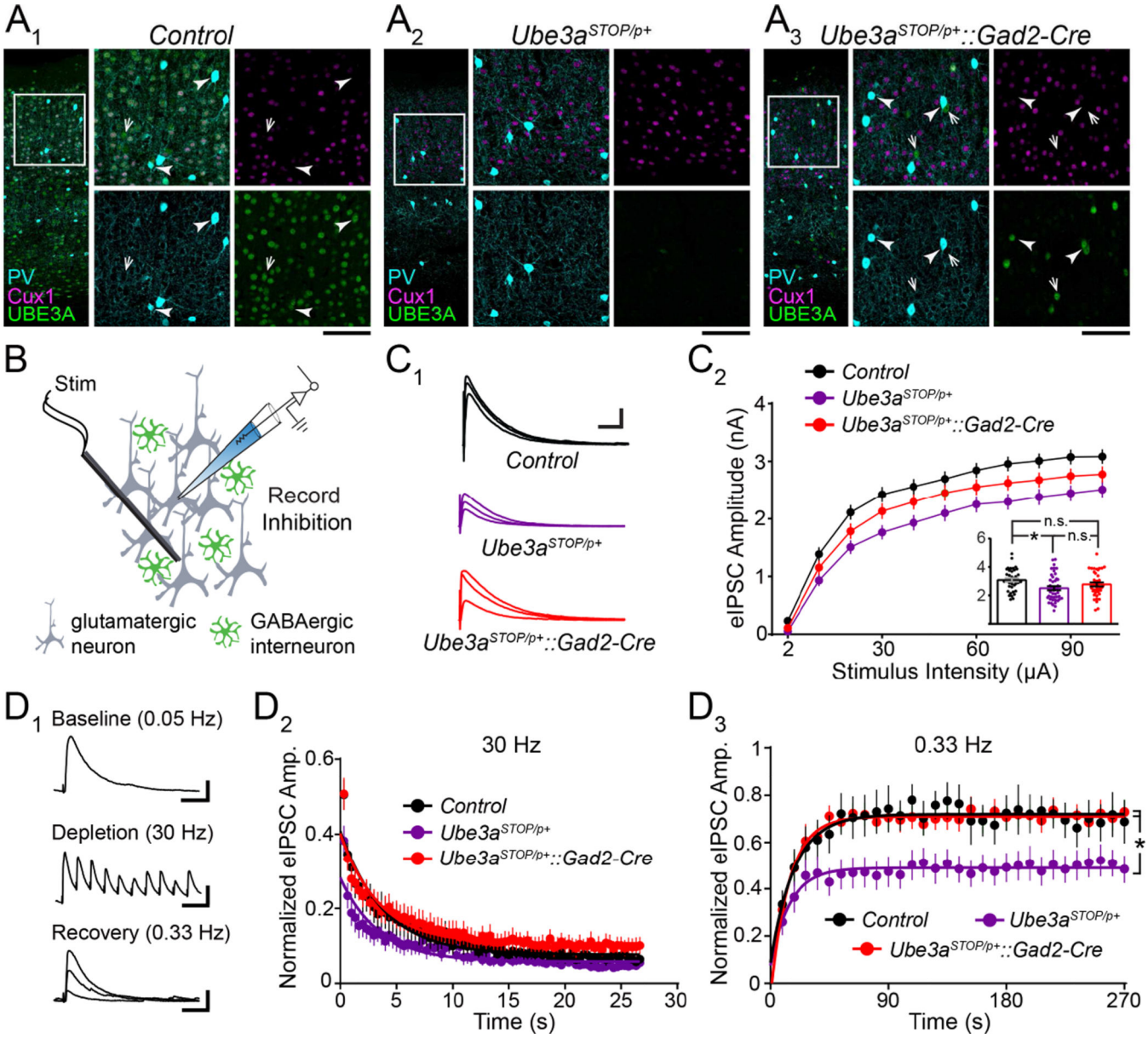


**Figure 2. GABAergic *Ube3a* reinstatement in *Ube3a*$^{STOP/p+}$*::Gad2-Cre* mice models glutamatergic *Ube3a* loss and indicates an evoked IPSC amplitude deficit onto L2/3 pyramidal neurons**

(**A**) Immunostaining of parvalbumin (PV), Cux1, and UBE3A in V1 of ~P80 *Control* ($A_1$), *Ube3a*$^{STOP/p+}$ ($A_2$), and *Ube3a*$^{STOP/p+}$*::Gad2-Cre* ($A_3$) mice. Arrowheads indicate PV-positive interneurons that co-stain for UBE3A. Arrows point to PV-negative interneurons that co-stain for UBE3A (scale bar = 145 μm or 75 μm for zoom-ins). (**B**) Schematic for recording synaptic inhibition onto L2/3 pyramidal neurons in V1 of ~P80 *Ube3a*$^{STOP/p+}$*::Gad2-Cre* mice. (**C**) Sample recordings of eIPSCs ($C_1$) at stimulation intensities of 2, 10, 30, and 100 μA (scale bar = 1 nA, 60 ms). ($C_2$) Quantification of eIPSCs. Inset depicts response amplitudes to 100 μA stimulation (*Control* n = 38 cells; *Ube3a*$^{STOP/p+}$ n = 44 cells; *Ube3a*$^{STOP/p+}$*::Gad2-Cre* n = 40 cells). (**D**) Inhibitory synaptic

depletion and recovery in *Control* (n = 9 cells), *Ube3a*$^{STOP/p+}$ (n = 11 cells), and *Ube3a*$^{STOP/p+}$*::Gad2-Cre* (n = 13 cells) mice, performed as in Figure 1E. Scale bars ($D_1$): baseline = 200 pA, 20 ms; depletion = 200 pA, 70 ms; recovery = 200 pA, 20 ms. Data represent mean ± SEM. *p≤0.05.

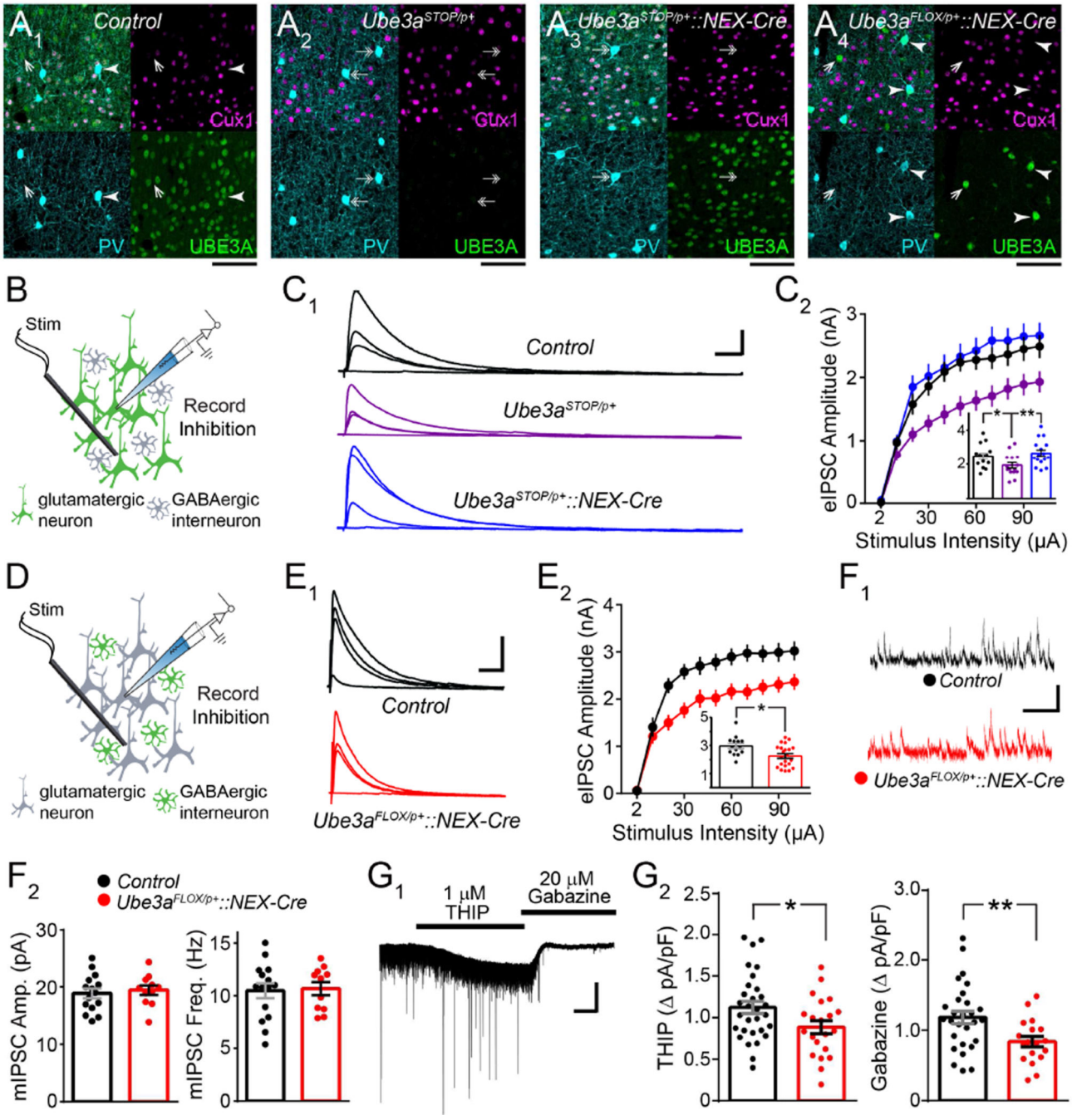


**Figure 3. Glutamatergic *Ube3a* loss selectively reduces evoked IPSC amplitude and tonic inhibitory tone onto L2/3 pyramidal neuron**

(**A**) Immunostaining of parvalbumin (PV), Cux1, and UBE3A in V1 of ~P80 *Control* ($A_1$), *Ube3a*$^{STOP/p+}$ ($A_2$), *Ube3a*$^{STOP/p+}$*::NEX-Cre* ($A_3$), and *Ube3a*$^{FLOX/p+}$*::NEX-Cre* ($A_4$) mice. Double arrows indicate PV-positive interneurons that lack UBE3A, arrowheads indicate PV-positive interneurons that co-stain for UBE3A but lack Cux1, and single arrows depict Cux1- and PV-negative interneurons that co-stain for UBE3A (scale bar = 75 μm for all panels). (**B**) Schematic for recording inhibition onto L2/3 pyramidal neurons in V1 of ~P80

*Ube3a*$^{STOP/p+}$*::NEX-Cre* mice. (**C**) Sample recordings of eIPSCs ($C_1$) at stimulation intensities of 2, 10, 30, and 100 μA (scale bar = 800 pA, 20 ms). ($C_2$) Quantification of eIPSCs. Inset depicts response amplitudes to 100 μA stimulation (*Control* n = 14 cells; *Ube3a*$^{STOP/p+}$ n= 15 cells; *Ube3a*$^{STOP/p+}$*::NEX-Cre* n = 16 cells). (**D**) Schematic for recording inhibition onto L2/3 pyramidal neurons in V1 of ~P80 *Ube3a*$^{FLOX/p+}$*::NEX-Cre* mice. (**E**) Sample recordings of eIPSCs ($E_1$) at stimulation intensities of 2, 10, 30, and 100 μA (scale bar = 1 nA, 40 ms). ($E_2$) Quantification of eIPSCs. Inset depicts response amplitudes to 80 μA stimulation (*Control* n = 14 cells; *Ube3a*$^{FLOX/p+}$*::NEX-Cre* n = 22 cells). (**F**) Sample recordings ($F_1$, scale bar = 20 pA, 200 ms) and quantification of mIPSC amplitude and frequency ($F_2$) (*Control* n = 15 cells; *Ube3a*$^{FLOX/p+}$*::NEX-Cre* n = 11 cells). (**G**) Representative trace ($G_1$) from experiments to measure tonic inhibitory currents onto L2/3 pyramidal neurons (scale bar = 150 pA, 120 s). ($G_2$) Quantification of change in $I_{holding}$ in response to the application of the δ-$GABA_A$R agonist THIP (left) and the subsequent chase with the competitive $GABA_A$R antagonist, Gabazine (right) (*Control* n = 30 cells; *Ube3a*$^{FLOX/p+}$*::NEX-Cre* n = 21 cells). Data represent mean ± SEM. *p≤0.05, **p≤0.01.

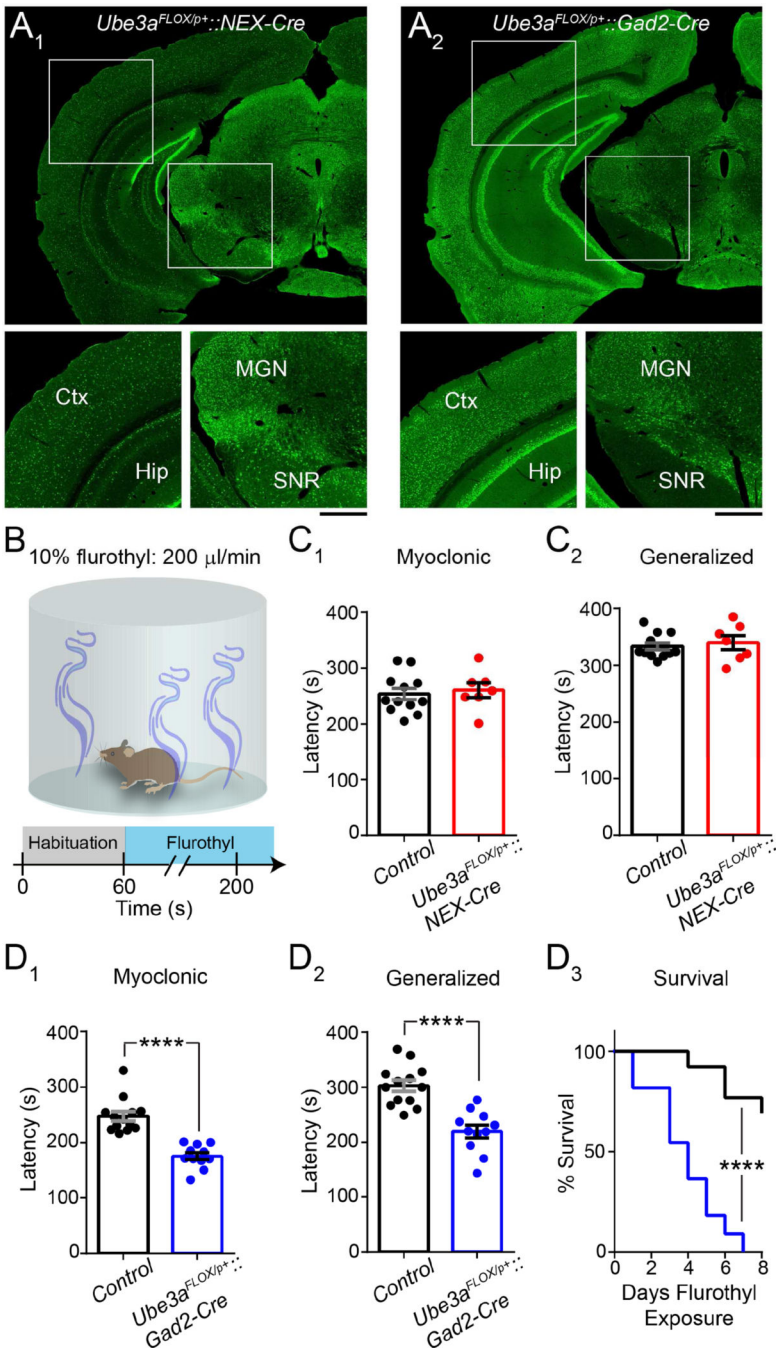


**Figure 4. GABAergic, but not glutamatergic *Ube3a* loss lowers the threshold for flurothyl-induced seizures**

(**A**) UBE3A staining in *Ube3a*$^{FLOX/p+}$*::NEX-Cre* ($A_1$) and *Ube3a*$^{FLOX/p+}$*::Gad2-Cre* ($A_2$) (scale bar = 750 μm; 400 μm for zoom-ins). Ctx, cerebral cortex; Hip, hippocampus; MGN, medial geniculate thalamic nucleus; SNR, substantia nigra pars reticulata. (**B**) Schematic of flurothyl-induced seizure protocol. Flurothyl administration ceases upon the occurrence of a generalized seizure. (**C**) Latency to myoclonus ($C_1$) and generalized seizure ($C_2$) in *Control* (n = 12) and *Ube3a*$^{FLOX/p+}$*::NEX-Cre* (n = 7) mice at ~P80. (**D**) Latency to myoclonus ($D_1$)

and generalized seizure ($D_2$) in *Control* (n = 13) and *Ube3a*$^{FLOX/p+}$*::Gad2-Cre* (n = 11) mice at ~P80. Comparative survival ($D_3$) of *Control* and *Ube3a*$^{FLOX/p+}$*::Gad2-Cre* mice following repeated once daily exposures to flurothyl. Data represent mean ± SEM. **** p≤0.0001.

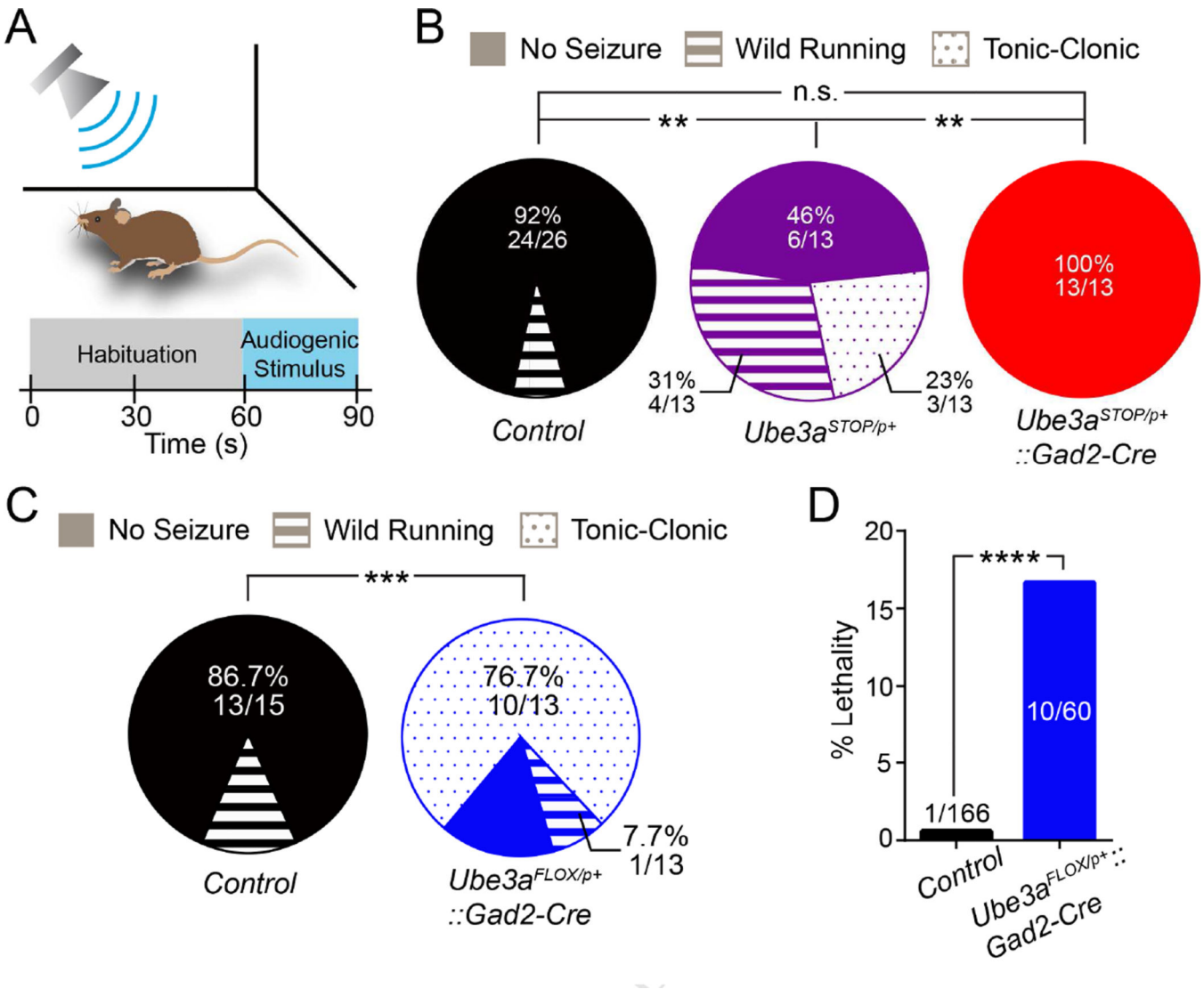


**Figure 5. GABAergic, but not glutamatergic, *Ube3a* loss enhances audiogenic seizure susceptibility in AS model mice**

(**A**) Schematic of audiogenic seizure protocol. (**B**) Quantification of audiogenic seizure susceptibility in *Control* (n = 26), *Ube3a*$^{STOP/p+}$ (n = 13), and *Ube3a*$^{STOP/p+}$*::Gad2-Cre* (n = 13) mice at ~P80. (**C**) Quantification of audiogenic seizure susceptibility (*Control* n = 15; *Ube3a*$^{FLOX/p+}$*::Gad2-Cre* n = 13). (**D**) Post-weaning (P21 – P90) lethality in *Control* and *Ube3a*$^{FLOX/p+}$*::Gad2-Cre* mice. Data represent mean ± SEM. **p≤0.01; ***p≤0.001; **** p≤0.0001.

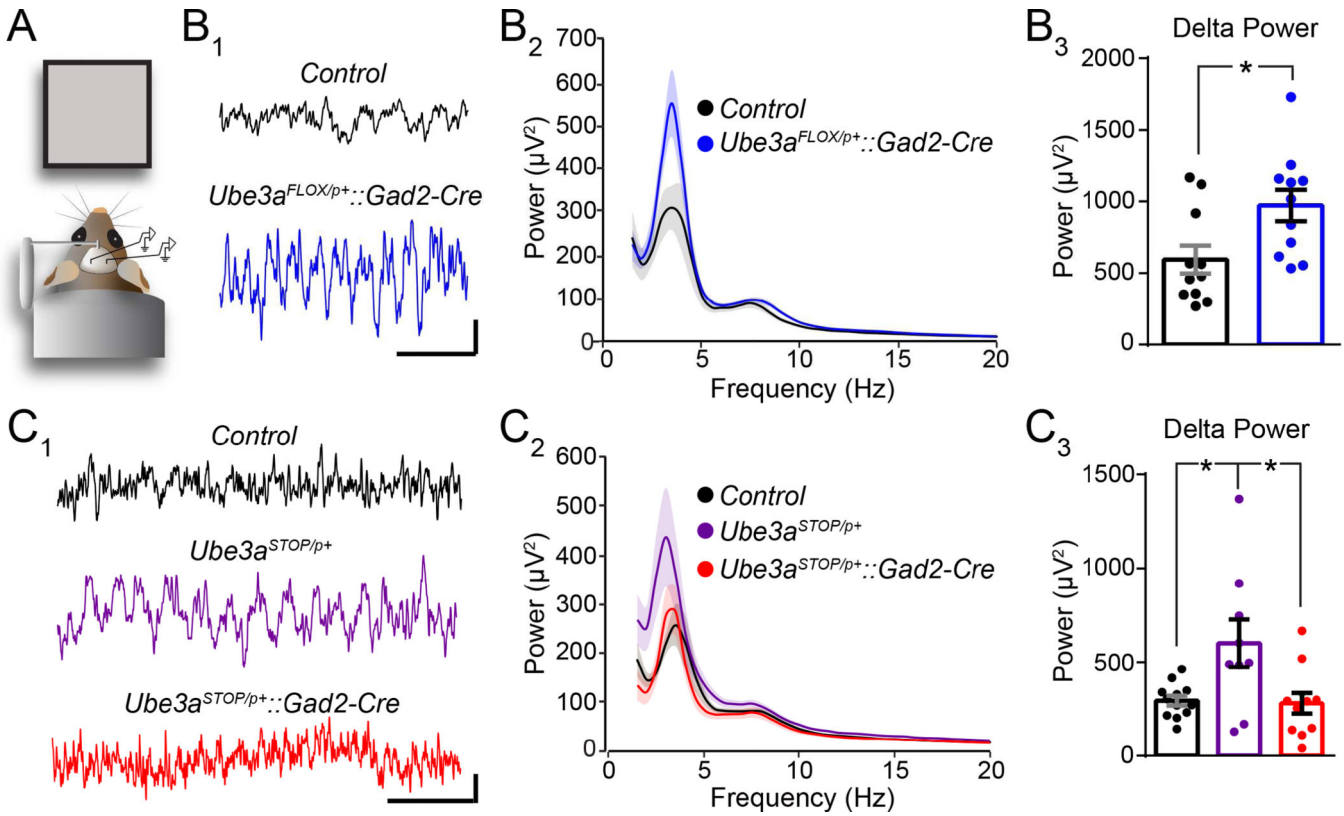


**Figure 6. GABAergic *Ube3a* loss selectively enhances LFP spectral power in the delta band**

(**A**) Schematized configuration for local field potential (LFP) recordings in non-anesthetized mice. (**B**) Sample V1 LFP recordings ($B_1$, scale bar = 100 μV, 1 s) and quantification of average spectral power ($B_2$) from *Control* (n = 11) and *Ube3a*$^{FLOX/p+}$*::Gad2-Cre* (n = 11) mice at ~P100. ($B_3$) Quantification of the region (3–4 Hz) encompassing the largest genotypic difference in power within the delta band. (**C**) Sample V1 LFP recordings ($C_1$, scale bar = 100 μV, 1 s) and quantification of average spectral power ($C_2$) from from *Control* (n = 12), *Ube3a*$^{STOP/p+}$ (n = 9), and *Ube3a*$^{STOP/p+}$*::Gad2-Cre* (n = 11) mice at ~P100. ($C_3$) Quantification of the region (2–3 Hz) encompassing the largest genotypic difference in power within the delta band. Data represent mean ± SEM. *p≤0.05.

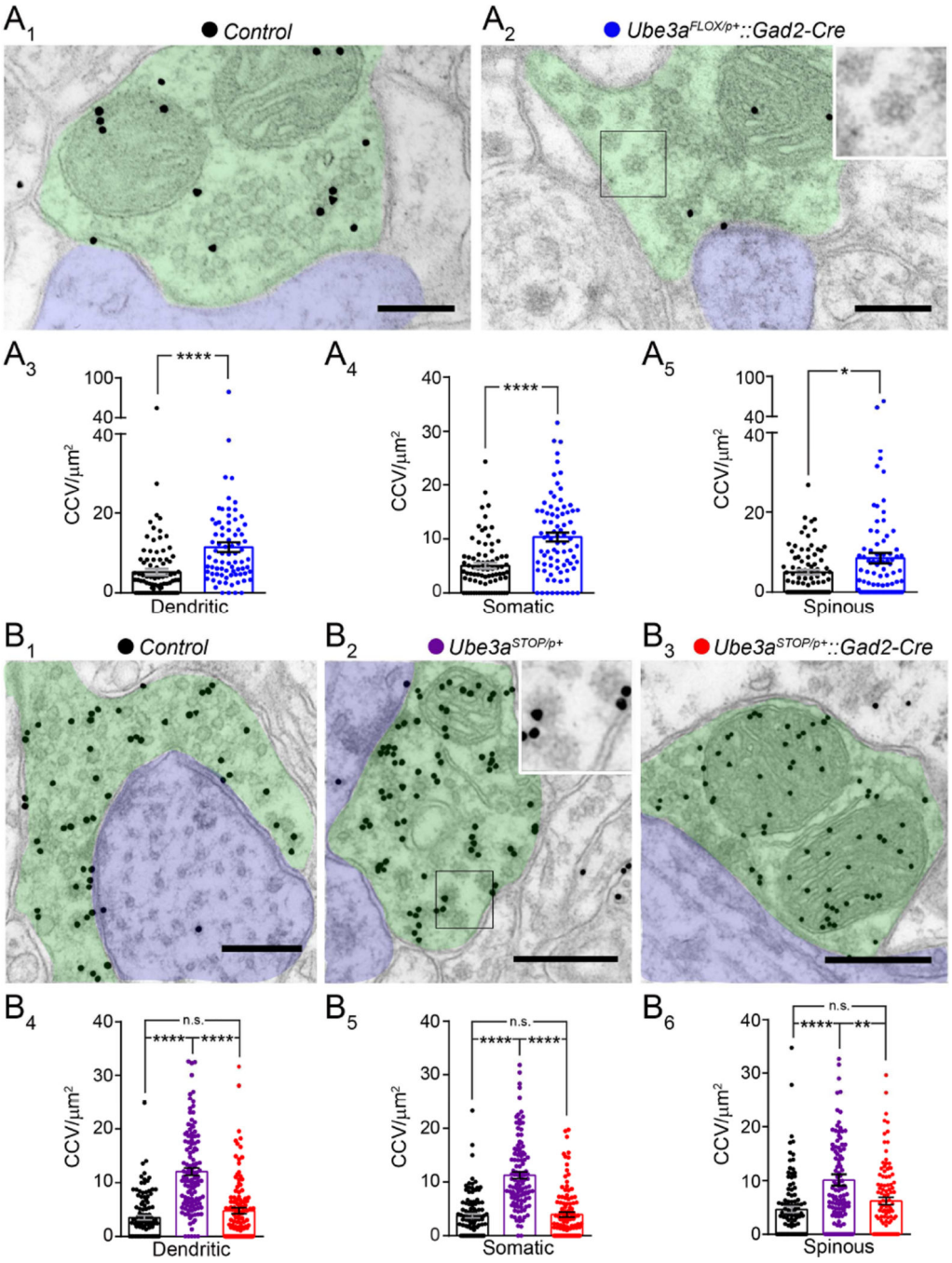


**Figure 7. GABAergic *Ube3a* loss underlies presynaptic CCV accumulation at both GABAergic and glutamatergic synapses**

(**A**) Electron micrographs of dendritic inhibitory synapses stained for GABA in *Control* ($A_1$) and *Ube3a*$^{FLOX/p+}$*::Gad2-Cre* ($A_2$) mice at ~P80. Green denotes GABAergic axon terminal, blue denotes dendrite, inset highlights clathrin-coated vesicles (CCVs) (scale bar = 200 nm). Average CCV densities at dendritic GABAergic synapses ($A_3$, *Control* n = 89 synapses from 3 mice; *Ube3a*$^{FLOX/p+}$*::Gad2-Cre* n = 77 synapses from 3 mice), somatic GABAergic synapses ($A_4$, *Control* n =78 synapses from 3 mice; *Ube3a*$^{FLOX/p+}$*::Gad2-Cre* n = 81

synapses from 3 mice), and spinous glutamatergic synapses ($A_5$, *Control* n = 82 synapses from 3 mice; *Ube3a*$^{FLOX/p+}$*::Gad2-Cre* n = 80 synapses from 3 mice). (**B**) Electron micrographs of dendritic inhibitory synapses stained for GABA in *Control* ($B_1$), *Ube3a*$^{STOP/p+}$ ($B_2$), and *Ube3a*$^{STOP/p+}$*::Gad2-Cre* ($B_3$) mice at ~P80. Green denotes GABAergic axon terminal, blue denotes dendrite, inset highlights clathrin-coated vesicles (CCVs) (scale bar = 400 nm). Average CCV densities at dendritic GABAergic synapses ($B_4$, *Control* n = 110 synapses from 3 mice; *Ube3a*$^{STOP/p+}$ n = 119 synapses from 3 mice; *Ube3a*$^{STOP/p+}$*::Gad2-Cre* n = 115 synapses from 3 mice), somatic GABAergic synapses ($B_5$, *Control* n = 103 synapses from 3 mice; *Ube3a*$^{STOP/p+}$ n = 114 synapses from 3 mice; *Ube3a*$^{STOP/p+}$*::Gad2-Cre* n = 110 synapses from 3 mice), and spinous glutamatergic synapses ($B_6$, *Control* n = 108 synapses from 3 mice; *Ube3a*$^{STOP/p+}$ n = 113 synapses from 3 mice; *Ube3a*$^{STOP/p+}$*::Gad2-Cre* n = 113 synapses from 3 mice). Data represent mean ± SEM. * $p<0.05$; ** $p<0.01$; **** $p<0.0001$.

*Neuron*. Author manuscript; available in PMC 2017 April 06.

**Table 1**

Summary of neocortical inhibitory synaptic defects, EEG abnormalities, and behavioral seizure phenotypes in *Ube3a* mice

| mouse model | maternal *Ube3a* expression deficit | GABAergic synaptic defects onto L2/3 pyramidal neurons | | | | intracortical EEG | behavioral seizure phenotype |
|---|---|---|---|---|---|---|---|
| | | mIPSC freq. | eIPSC amp. | inhibitory synaptic recovery | inhibitory presynaptic CCVs | | |
| *Ube3a*$^{m-/p+}$ | deleted in all neurons | [a]↓49% | [a]↓43% | [a]↓30% | [a]↑214% | [b]electrographic seizures, polyspike and slow wave discharges | spontaneous: [b]yes<br>flurothyl: NA<br>AGS: [bc]enhanced susceptibility |
| *Ube3a*$^{FLOX/p+}$ *Nestin-Cre* | deleted in all neurons | ↓25% | ↓18% | ↓18% | ↑124% | NA | NA |
| *STOP/p+ Ube3a* | suppressed in all neurons | ↔ | ↓20% | ↓32% | ↑222% | enhanced delta power | spontaneous: not observed<br>flurothyl: NA<br>AGS: [d]enhanced susceptibility |
| *Ube3a*$^{FLOX/p+}$ *Gad2-Cre* | deleted in nearly all GABAergic neurons | ↔ | ↔ | ↔ | ↑116% | enhanced delta power | spontaneous: yes, enhanced postnatal lethality<br>flurothyl: decreased latency, enhanced lethality<br>AGS: enhanced susceptibility, severe |
| *Ube3a*$^{STOP/p+}$ *Gad2-Cre* | suppressed in all glutamatergic neurons and other non-GABAergic neurons | ↔ | [e]↓10% | ↔ | ↔ | normalized delta power | spontaneous: not observed<br>flurothyl: NA<br>AGS: not susceptible |
| *Ube3a*$^{FLOX/p+}$ *NEX-Cre* | deleted in glutamatergic neurons of dorsal pallial origin | ↔ | ↓25% | ↔ | NA | NA | spontaneous: not observed<br>flurothyl: normal susceptibility<br>AGS: NA |

↔, equivalent to Control; ↑, increased relative to Control; ↓, decreased relative to Control; NA, Not Assayed; AGS, audiogenic seizure;

[a]Wallace et al., 2012;

[b]Jiang et al., 1998;

[c]van Woerden et al., 2007;

[d] Silva-Santos et al., 2015;

[e] did not reach statistical significance.